

Quantum error thresholds for gauge-redundant digitizations of lattice field theories

Marcela Carena,^{1,2,3,4,*} Henry Lamm,^{1,†} Ying-Ying Li,^{5,6,‡} and Wanqiang Liu^{4,§}

¹*Fermi National Accelerator Laboratory, Batavia, Illinois, 60510, USA*

²*Enrico Fermi Institute, University of Chicago, Chicago, Illinois, 60637, USA*

³*Kavli Institute for Cosmological Physics, University of Chicago, Chicago, Illinois, 60637, USA*

⁴*Department of Physics, University of Chicago, Chicago, Illinois, 60637, USA*

⁵*Peng Huanwu Center for Fundamental Theory, Hefei, Anhui 230026, China*

⁶*Interdisciplinary Center for Theoretical Study, University of Science and Technology of China, Hefei, Anhui 230026, China*

(Dated: February 27, 2024)

In the quantum simulation of lattice gauge theories, gauge symmetry can be either fixed or encoded as a redundancy of the Hilbert space. While gauge-fixing reduces the number of qubits, keeping the gauge redundancy can provide code space to mitigate and correct quantum errors by checking and restoring Gauss's law. In this work, we consider the correctable errors for generic finite gauge groups and design the quantum circuits to detect and correct them. We calculate the error thresholds below which the gauge-redundant digitization with Gauss's law error correction has better fidelity than the gauge-fixed digitization. Our results provide guidance for fault-tolerant quantum simulations of lattice gauge theories.

I. INTRODUCTION

Gauge symmetries in quantum field theories give rise to extremely rich phenomena. Most prominently, $SU(3) \times SU(2) \times U(1)$ gauge symmetry describes the interactions of the Standard Model. Making ab initio predictions for comparison to experiment requires large computational resources. In particular, Monte Carlo methods in lattice gauge theory (LGT) have been fruitful in the past couple of decades, thanks to the advancement of supercomputers and algorithms. However, problems involving dynamics such as out-of-equilibrium evolution in the early universe [1–4], transport coefficients of the quark-gluon plasma [5] and parton physics in hadron collisions [6–11] present sign problems, as the Boltzmann weight becomes complex-valued. Future, large-scale quantum computers can avoid this obstacle by performing real-time simulations in the Hamiltonian formalism [12–15].

In order to use quantum computers for simulations, the infinite-dimensional Hilbert space of the gauge theory must be addressed. To allow a mapping to a finite quantum memory, many digitization proposals to truncate this space have been studied (see Sec VI.b of [15]). All truncations break the continuous symmetries to some degree and produce theories with smaller symmetries. Understanding the theoretical errors introduced by this is an area of active research [16–22]. Broadly speaking, methods to encode these regularized theories in quantum computers fall into two classes. The first class digitizes all the states connected through gauge transformations as *redundancy* and uses Gauss's law to project the gauge-invariant subspace, where the physical theory should be simulated. This can be done in group element basis [18, 23–31], the group

representation basis [23, 32–37], the mixed basis [38], as a fuzzy gauge theory [39, 40], as a quantum link model [41–44], and more. The second class digitizes only gauge-invariant states. We refer to this as *fixing the gauge* in the sense that it eliminates the redundant degrees of freedom. One can digitize the independent Wilson loops in the lattice, which can be identified as the plaquettes in $(2+1)$ dimensions [45–52], and as the states outside the maximal tree in higher dimensions [20]. Other digitizations to eliminate redundancy include the Fock basis in the light-front Hamiltonian [7, 53], the local multiplet basis [54, 55], and spin networks [56, 57]. Besides reducing the qubit cost, gauge fixing also simplifies the quantum state preparation, but can complicate the Hamiltonian [20, 45, 54–63]. At present, it is an open question whether gauge fixing is ultimately advantageous for quantum simulation.

The effect of noisy hardware has been generally neglected in the above discussion. Naively, gauge-redundant digitizations suffer more severely from quantum noise because more qubits introduce more errors. However, not all the errors are equally harmful. Noise which breaks symmetries can change the universality class simulated [35, 36, 39, 64–66] and thus sufficient symmetry preservation is crucial [61, 67–71]. In the gauge-redundant digitization, quantum errors can be classified as gauge-preserving or gauge-violating operators [71–76]. The gauge-violating errors can be mitigated by introducing energy penalties [77–81] or random gauge transformations [68] in the Hamiltonian evolution. They can also be corrected by measuring and restoring Gauss's law [67, 82]. The gauge-fixed digitization – while precluded from noise-based gauge violations – does not have such natural error mitigation or correction methods, and thus relies on generic methods for the residual errors.

Notably, redundancy and symmetry play a central role in both quantum error correction (QEC) and mitigation (QEM). QEC deliberately designs a redundant full Hilbert space $\mathcal{H}_{\text{full}}$ on the physical qudits and encodes quantum information in a much smaller code subspace $\mathcal{H}_{\text{code}}$ on

* carena@fnal.gov

† hlammm@fnal.gov

‡ yingyingli@ustc.edu.cn

§ wanqiangli@uchicago.edu

logical qudits with certain symmetries, thus allowing for correction without disrupting the coherent quantum information in $\mathcal{H}_{\text{code}}$ [83, 84]. As an active field of research, estimates for the overhead – the physical to logical qubit ratio – vary from $\mathcal{O}(10)$ to $\mathcal{O}(10^5)$ [85–87]. QEM uses the existing symmetries without introducing redundancy to mitigate errors [88]. Indeed, it is this structural similarity between QEC, QEM and LGT that inspires the above mentioned works [67–72, 74–77, 81, 82] to use gauge redundancy as a resource for error correction and mitigation. Given the huge variance of the overhead in QEC, and that gauge fixing saves logical qubits only by a factor of approximately $(1 - 1/d)$ in d spatial dimensions, keeping the gauge redundancy for QEC or QEM may be more resource efficient for achieving a desired accuracy. This idea has only just begun to be explored for field theories [76, 89–91] including fermionic systems [92, 93].

The answer to *when* this is true can be phrased as a *threshold theorem* of QEC [94–96], which states that there is a threshold for the error rate of physical qubits, below which more redundancy makes the code more error-proof. In this work, we compute the threshold below which gauge redundancy makes the digitization more robust. After reviewing the connection between gauge symmetry and QEC in Sec. II and Sec. III, we present the circuits to encode and decode via Gauss’s law. This paves the way for calculations in Sec. IV of the thresholds, below which the gauge-redundant digitization combined with QEC has a better fidelity than the gauge-fixed one.

II. GAUGE SYMMETRY AND FIXING

We will briefly review gauge symmetry on lattice in both the group element (magnetic) and the group representation (electric) basis, as the former is closer to the path-integral quantization and the latter to Gauss’s law in classical fields. These bases are related by the group Fourier transform. In the group element basis, one assigns an element of the group G (link variable) to each link on the lattice, representing the Wilson line [97]. For continuous gauge groups, the link variables are related to the vector potentials of the continuum theory via:

$$U_{\mathbf{x},i} = P \exp(-i \int_{\mathbf{x}}^{\mathbf{x}+\mathbf{i}} d\mathbf{l} \cdot \mathbf{A}) \approx e^{-iaA_i(\mathbf{x})}, \quad (1)$$

where P denotes path ordering, a is the lattice spacing, and i the spacial direction of the link. The gauge-redundant Hilbert space $\mathcal{H}_{\text{gauge}}$ is the tensor product of N_L local spaces, each spanned by the group elements:

$$\mathcal{H}_{\text{gauge}} = \text{span}(\{|U\rangle, U \in G\})^{\otimes N_L} \quad (2)$$

where N_L is the total number of links and $\langle U|U'\rangle = \delta_{U',U}$.

For a continuous gauge group, $\dim(\mathcal{H}_{\text{gauge}}) = \infty$, and digitization is required to render it finite. Here we will focus on the discrete subgroup digitization. Some discussion of the continuous theory can be found in [98] and

other digitization schemes remain for future works. For a discrete gauge group G , the dimension of the one-link Hilbert space is $|G|$. The dimension of $\mathcal{H}_{\text{gauge}}$ is given by:

$$\dim \mathcal{H}_{\text{gauge}} = |G|^{N_L}. \quad (3)$$

A gauge transformation $\hat{T}_{g_{\mathbf{x}}}$ is a unitary operator that transforms all out-going (in-coming) links connected to a site \mathbf{x} by a left (right) product with $g \in G$ ($g^{-1} \in G$):

$$\hat{T}_{g_{\mathbf{x}}} = \prod_{i=1}^d [\hat{L}_g(\mathbf{x}, i) \hat{R}_{g^{-1}}(\mathbf{x} - \mathbf{i}, i)], \quad (4)$$

where \hat{L}_g, \hat{R}_g are left and right multiplication operators,

$$\hat{L}_g = \sum_{U \in G} |gU\rangle \langle U|, \quad \hat{R}_{g^{-1}} = \sum_{U \in G} |Ug^{-1}\rangle \langle U|. \quad (5)$$

Typical lattice gauge Hamiltonians preserves gauge symmetry as they commutes with the gauge transformation operator $\hat{T}_{g_{\mathbf{x}}}$. This includes the Kogut-Susskind [97], the Symanzik-improved [99–102] and the Similarity-Renormalization-Group-improved ones [21].

Gauge-invariant states satisfy a lattice version of Gauss’s law:

$$\hat{T}_{g_{\mathbf{x}}} |\Psi_{\text{inv}}\rangle = |\Psi_{\text{inv}}\rangle, \quad \forall g_{\mathbf{x}} \in G. \quad (6)$$

In the $|U\rangle$ basis, Gauss’s law requires the wave functions on gauge-equivalent configurations to be the same, as taking an inner product of Eq. (6) with $\langle U|$ gives

$$\langle U | \hat{T}_{g_{\mathbf{x}}} | \Psi_{\text{inv}} \rangle = \langle U | \Psi_{\text{inv}} \rangle \quad (7)$$

Such states are in the gauge-invariant subspace \mathcal{H}_{inv} , which can be projected from $\mathcal{H}_{\text{gauge}}$ with the operator $\hat{P}_{\text{inv}} \equiv \prod_{\mathbf{x}} \hat{P}_0(\mathbf{x})$, where the local Gauss’s law projector is

$$\hat{P}_0(\mathbf{x}) = \frac{1}{|G|} \sum_{g_{\mathbf{x}} \in G} \hat{T}_{g_{\mathbf{x}}}. \quad (8)$$

To get a clearer physical picture, it is useful to introduce the electric basis $|\sigma_{mn}\rangle$, which is the group Fourier transform of the group element basis:

$$\langle \sigma_{mn} | U \rangle = \sqrt{d_{\sigma}/|G|} \Gamma_{mn}^{(\sigma)}(U), \quad (9)$$

where $\Gamma_{mn}^{(\sigma)}(U)$ is the m, n matrix element of the unitary irreducible representation (irrep) σ for U , d_{σ} is the dimension of σ . The dimension of the one-link Hilbert space $|G|$ also equals $\sum_{\sigma} d_{\sigma}^2$. For the Abelian groups, all irreps are 1d and m, n can therefore be suppressed with σ being the Abelian electric flux. For non-Abelian groups, $|\sigma_{mn}\rangle$ is a tensor representation comprised of the left vector representation $|\sigma_m\rangle$ and the right vector representation $|\bar{\sigma}_n\rangle$:

$$|\sigma_{mn}\rangle = |\sigma_m\rangle \otimes |\bar{\sigma}_n\rangle, \quad (10)$$

where $\bar{\sigma}$ is the complex conjugate dual of representation σ , i.e. $\Gamma_{nq}^{(\bar{\sigma})}(g) = \Gamma_{qn}^{(\sigma)}(g^{-1})$. This is because gauge transformations act on the links going out from the vertex via

$$\hat{L}_g = \sum_{\sigma,m,q} \Gamma_{mq}^{(\sigma)}(g) |\sigma_m\rangle \langle \sigma_q| \otimes \sum_n |\bar{\sigma}_n\rangle \langle \bar{\sigma}_n|, \quad (11)$$

thus transforming only the left vector. Similarly, the incoming links transform in the dual representation, and only the right vectors are transformed:

$$\hat{R}_{g^{-1}} = \sum_{\sigma,m} |\sigma_m\rangle \langle \sigma_m| \otimes \sum_{n,q} \Gamma_{nq}^{(\bar{\sigma})}(g) |\bar{\sigma}_n\rangle \langle \bar{\sigma}_q|. \quad (12)$$

Thus, one can define the local charge at vertex \mathbf{x} as the tensor product representation:

$$|Q(\mathbf{x})\rangle = \prod_{i=1}^d \otimes |\sigma_m(\mathbf{x}, i)\rangle \otimes |\bar{\sigma}_n(\mathbf{x} - \mathbf{i}, i)\rangle \quad (13)$$

$\hat{P}_0(\mathbf{x})$ projects the tensor product to the trivial representation according to the Clebsch-Gordan coefficients of the group. Physically, one can interpret $Q(\mathbf{x})$ as the net flux, and $\hat{P}_0(\mathbf{x})$ selects states with neutral net flux. As the result of the constraints, one lacks the freedom to independently assign all the links variables. Naively, applying $\hat{P}_0(\mathbf{x})$ to all the N_V vertices in the lattice implies N_V different constraints. However, the global charge, defined as the tensor product of all the local charges,

$$|Q_{\text{gl}}\rangle = \prod_{\mathbf{x}} \otimes |Q(\mathbf{x})\rangle = \prod_{\mathbf{x},i} \otimes |\sigma_m(\mathbf{x}, i)\rangle \otimes |\bar{\sigma}_n(\mathbf{x}, i)\rangle \quad (14)$$

is not a gauge constraint but rather the physically-conserved charge of the state under the global transformation with $h \in G$:

$$\hat{T}_h^{\text{Gl}} \prod_{\mathbf{x},i} |U_{\mathbf{x},i}\rangle = \prod_{\mathbf{x},i} |hU_{\mathbf{x},i}h^{-1}\rangle. \quad (15)$$

In the case of an Abelian group like $U(1)$ or \mathbb{Z}_N , the links cannot carry charge as the charges of the left and right vector always cancel, making the global charge automatically neutral. This can also be easily seen in the group element basis as all states are invariant under Eq. (15). In contrast, non-Abelian gauge fields can carry charge, as indicated by the difference between the left and right vectors, and the non-trivial global transformations. If one allows for all the possible global charges, the number of independent constraints is thus $N_V - 1$. This makes $N_L - N_V + 1$ links dynamical with the rest $N_V - 1$ links dependent on the dynamical ones. Thus,

$$\dim \mathcal{H}_{\text{inv}} = |G|^{N_L - N_V + 1}. \quad (16)$$

If one fixes the global transformations as well, thereby selecting the subspace with neutral global charge, the dimension of \mathcal{H}_{inv} might be reduced by a factor greater

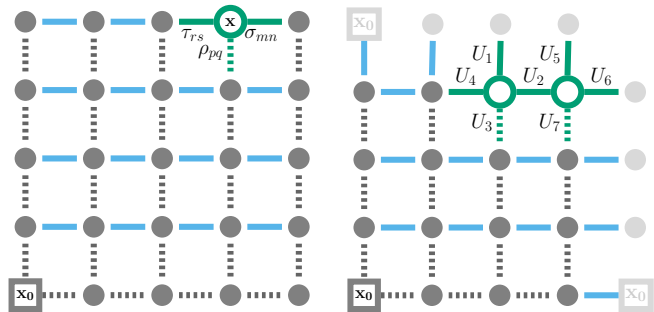


FIG. 1. Maximal trees (dashed lattice links) of lattices with (left) OBC and (right) PBC. The site at the lower left corner is chosen as the root of the maximal tree.

or equal to $|H|/|G|$ where H is the Abelian center of the group, as derived in Appendix A.

Choosing which degrees of freedom are independent and eliminating others is equivalent to gauge fixing. On the lattice, the maximal tree method fixes the gauge up to the global transformations Eq. (15), by explicitly solving the local Gauss's law constraints which forces some links to be functions of the remaining ones (See [103] for a good discussion). For example, consider the links connected to the vertex \mathbf{x} shown in the left of Fig. 1, the state are given by ¹

$$|\Psi_{\text{gauge}}\rangle = \sum_{\sigma,\rho,\tau} a(\sigma, \rho, \tau) |\sigma, \rho, \tau\rangle. \quad (17)$$

Constraining $|Q(\mathbf{x})\rangle$ to be in the trivial representation, the variable ρ in the maximal tree can be determined as $\rho = \sigma \otimes \bar{\tau}$, which produces the gauge-invariant state:

$$|\Psi_{\text{inv}}\rangle = \sum_{\sigma,\tau} a(\sigma, \tau) |\sigma, \tau\rangle \otimes |\rho = \sigma \otimes \bar{\tau}\rangle. \quad (18)$$

The same procedure can be repeated till the dependent links form a maximal tree in the lattice, i.e. a set of links which contains one and only one path between any pair of vertices, the size of which is $N_T = N_V - 1$. We will define the Hilbert space spanned by the variables completely determined by Gauss law (in the maximal tree in the above example) as \mathcal{H}_{red} , and the rest as $\mathcal{H}_{\text{fixed}}$. Clearly,

$$\mathcal{H}_{\text{inv}} \cong \mathcal{H}_{\text{fixed}} = \text{span}(\{|U\rangle, U \in G\})^{\otimes N_L - N_V + 1}. \quad (19)$$

Similar to choice of gauge fixing in the continuum, for a given lattice there is no unique maximal tree. One popular method [20, 104–106] is to pick a site \mathbf{x}_0 , and the set of links which uniquely connects \mathbf{x}_0 via a comb-like path to any other site form a tree of size $N_T = N_V - 1$. This maximal tree is shown in Fig. 1 for 2d with open (OBC) and periodic (PBC) boundary conditions. Notably,

¹ We have suppressed the vector indices of representations here for simplicity.

the charge at \mathbf{x}_0 is not fixed by the maximal tree, but left to carry the charge under global transformations in Eq. (15) [20, 106].

In the *gauge-redundant* quantum simulations digitized with Hilbert space $\mathcal{H}_{\text{gauge}}$ and a quantum computer made of qudits of dimension N , the number of qudits required is $\log_N(\dim \mathcal{H}_{\text{gauge}}) = N_L \log_N |G|$. *Gauge fixing* eliminates the redundancy by digitizing the subspace \mathcal{H}_{inv} instead, thus reducing the number of qudits to $\log_N(\dim \mathcal{H}_{\text{inv}})$. For the rest of the work, we take $\log_N(\dim \mathcal{H}_{\text{inv}}) \approx (N_L - N_T) \log_N |G|$, which is accurate for fixing the maximal tree in both the Abelian and non-Abelian cases, and an upper bound for non-Abelian G if the global symmetry is also fixed. The numbers of sites, links, links in a maximal tree are listed in Tab. I for different boundary conditions.

TABLE I. The number of degrees of freedom in a lattice with L links per side in d dimensions. $b = 0, 1$ for PBC and OBC respectively.

Sites N_V	$(L + b)^d$
Links N_L	$dL(L + b)^{d-1}$
Maximal Tree Links N_T	$(L + b)^d - 1$

Gauge fixing reduces the number of qubits, but often at the price of complicating the lattice gauge Hamiltonian \hat{H}_{LGT} . Written with the gauge-redundant degrees of freedom, \hat{H}_{LGT} only consists of local electric and magnetic energy operators. In the gauge-fixed formalism with Hamiltonian \hat{H}_{fixed} , the electric operators of the redundant links in the maximal tree cannot be discarded, but are non-local combinations of operators outside the tree [20, 106]. Thus \hat{H}_{fixed} is generically denser and non-local. It is easier to fix the gauge while keeping the Hamiltonian simple in 1d or 2d. In 2d, $\log_{|G|} \dim \mathcal{H}_{\text{inv}}$ is

$$N_L - N_T = N_L - N_V + 1 = N_P - \chi + 1, \quad (20)$$

where N_P is the number of plaquettes, and χ is the Euler characteristic. This also follows from counting the number of plaquettes with independent magnetic fluxes (Wilson loops), plus the topological degrees of freedom. For an OBC lattice ($\chi = 1$), all N_P plaquettes are independent and there are no topological degrees of freedom. This plaquette magnetic flux basis keeps the Hamiltonian local and sparse for Abelian gauge groups [38, 45–52]. For a PBC lattice ($\chi = 0$), the total magnetic flux is zero, thus there are $(N_P - 1)$ plaquettes with independent magnetic fluxes. Additionally, considering the two independent Wilson loops with winding number one, this yields $\dim \mathcal{H}_{\text{inv}} = |G|^{N_P+1}$.

III. LATTICE GAUGE SYMMETRIES AS STABILIZER CODES

In this section, we construct quantum circuits to use gauge redundancy as partial error correction codes for

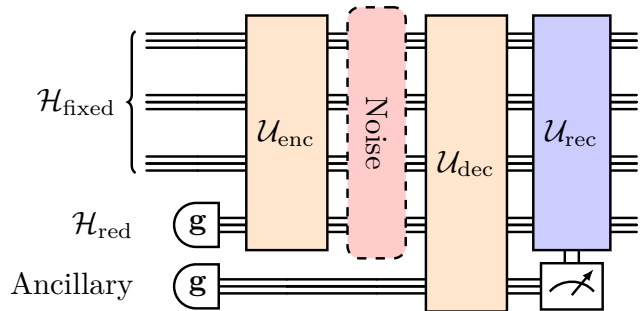


FIG. 2. Schematic circuit of LGT as QEC. \mathbf{g} represents a color-neutral state.

generic finite groups. The method is based on the similarity between stabilizer codes and lattice gauge theories, which we review in III.1. Without redundancy, any error in $\mathcal{H}_{\text{fixed}}$ causes irrecoverable information loss. In the gauge-redundant formalism, as a result of gauge symmetry Eq. (7), all the states equivalent under gauge transformation carry copies of the same wave function. This allows one to detect and correct some gauge-symmetry violating errors, as is analyzed in III.2. Fig. 2 outlines the circuit to realize such error corrections. The preparation of gauge invariant states is a process to encode the quantum information with the maximal-tree redundancy. To decode, we introduce an ancillary register at each site to compute and measure the net flux. Nonzero fluxes indicates occurrence of quantum errors which can be mitigated via post-selection, with the associated sampling overhead exhibiting exponential growth in the system size [107]. One can also correct these errors by applying the optimal recoveries after deducing the most likely errors. The details of the construction are in III.3.

III.1. Stabilizer codes

Stabilizer codes perform error correction by using a redundant *full Hilbert space* $\mathcal{H}_{\text{full}}$ of physical qubits (qudits), but encoding quantum information only in states with certain symmetries. The symmetry group that defines the code states is called the stabilizer group \mathcal{S} , usually a subgroup of the (generalized) Pauli group on the physical qubits (qudits). A code state satisfies

$$\hat{s} |\psi\rangle_{\text{code}} = |\psi\rangle_{\text{code}}, \forall \hat{s} \in \mathcal{S}. \quad (21)$$

All code states are in the *code space*, $\mathcal{H}_{\text{code}}$. The sum of all \hat{s} is proportional to the projector from $\mathcal{H}_{\text{full}}$ to $\mathcal{H}_{\text{code}}$:

$$\hat{P}_{\text{code}} = \frac{1}{|\mathcal{S}|} \sum_{\hat{s} \in \mathcal{S}} \hat{s}. \quad (22)$$

Note that Eq. (21) is similar to Eq. (6), and Eq. (22) to Eq. (8). Applying the above concepts to LGT, the group of gauge transformations \mathcal{G} is a stabilizer group,

and \mathcal{H}_{inv} corresponds to the code space. The projection operator \hat{P}_{inv} from $\mathcal{H}_{\text{gauge}}$ to \mathcal{H}_{inv} is the (normalized) sum of all stabilizers.² Measuring whether and how gauge symmetry is violated allows one to detect and correct gauge-violating errors.

In active QEC, one measures a minimum generating set of \mathcal{S} , and the results are *syndromes*. To avoid collapsing the quantum information in the measurement of syndromes, ancillae are needed to compute the syndromes coherently:

$$\left[\sum_X \psi(X) |X\rangle \right] \otimes |0\rangle_{\text{anc}} \rightarrow \sum_X \psi(X) |X\rangle \otimes |s(X)\rangle_{\text{anc}}, \quad (23)$$

where $|X\rangle$ are base vectors of the physical qubits. In the case of Pauli stabilizers with eigenvalue ± 1 , measuring the ancillary qubits collapses the state to $\mathcal{H}_{\text{code}}$ when all syndromes return $+1$, or one of the subspaces orthogonal to $\mathcal{H}_{\text{code}}$ if some syndromes return -1 indicate the errors. One then applies an optimal recovery operation to the quantum state depending on the syndromes. Clearly, errors that transform one state to another within $\mathcal{H}_{\text{code}}$ are not detectable, and those are *logical errors*.

The *code distance* is the minimum number of single physical qubit (qudit) errors that are part of a logical error. For scalable quantum error correction codes, which imply that the code distance can be arbitrarily large, there exists an *error threshold* for the error rate per physical qudit. If the physical error rate is below such threshold, we can decrease the logical error rate by increasing the code distance, despite the increased total errors due to more physical qudits [94–96].

III.2. The set of correctable errors

For a quantum system represented as a density operator ρ , the general noisy evolution can be written as a completely positive, trace-preserving map $\mathcal{N}(\rho)$:

$$\mathcal{N}(\rho) = \sum_j \hat{N}_j \rho \hat{N}_j^\dagger \quad (24)$$

where \hat{N}_j are error operators, usually including the identity operator. The necessary and sufficient condition for correctable errors is the Knill-Laflamme (KL) condition [108]:

$$\hat{P}_{\text{code}} \hat{N}_i^\dagger \hat{N}_j \hat{P}_{\text{code}} = \lambda_{ij} \hat{P}_{\text{code}}, \quad \lambda_{ij}^* = \lambda_{ji}. \quad (25)$$

For errors as operators on a G -register, a linearly independent complete basis can be constructed as $\{\hat{L}_g \hat{\Gamma}_\sigma\}$, where \hat{L}_g is the group left multiplication operator defined in Eq. (5), and $\hat{\Gamma}_\sigma$ is the matrix element operator:³

$$\hat{\Gamma}_{\sigma,m,n} = \sum_{h \in G} \sqrt{d_\sigma} \Gamma_{mn}^{(\sigma)}(h)^* |h\rangle \langle h| \quad (26)$$

One can check that the above set of operators are linearly independent by satisfying:

$$\text{Tr} [(\hat{L}_g \hat{\Gamma}_\sigma)^\dagger (\hat{L}_{g'} \hat{\Gamma}_{\sigma'})] = |G| \delta_{g,g'} \delta_{\sigma,\sigma'}. \quad (27)$$

The basis is complete as there are only $|G|^2$ independent operators in a Hilbert space of dimension $|G|$.

The gauge-violating effect of $\hat{\Gamma}_\sigma$ is clearer in the electric basis. Using Eq. (D1) between Clebsch-Gordan coefficients and the matrix elements of irreps in [109], one can derive:

$$\langle \sigma''_l | \hat{\Gamma}_{\sigma,m,n} | \sigma'_k \rangle = \sqrt{\frac{d_\sigma d_{\sigma'}}{d_{\sigma''}}} \sum_\alpha \langle \sigma''_l, \alpha | \sigma'_k, \sigma_m \rangle \langle \bar{\sigma}''_r, \alpha | \bar{\sigma}'_q, \bar{\sigma}_n \rangle, \quad (28)$$

where $\langle \sigma''_l, \alpha | \sigma'_k, \sigma_m \rangle$ is the Clebsch-Gordan coefficient, and the sum of α is from 1 to the multiplicity $M(\sigma''; \sigma', \sigma)$, i.e. the number of times that σ'' appears in the direct sum decomposition of the tensor product of σ and σ' . This can be interpreted as $\hat{\Gamma}_{\sigma,m,n}$ adding σ_m to the left vector and $\bar{\sigma}_n$ to the right vector. Thus, $\hat{\Gamma}_{\sigma,m,n}(\mathbf{x}, i)$ on a gauge-invariant state creates net flux σ_m at site \mathbf{x} and $\bar{\sigma}_n$ at the site $(\mathbf{x} + \mathbf{i})$. Applying $\hat{\Gamma}_{\sigma,m,n}^\dagger$ to the same link annihilates the flux and restores gauge symmetry. Indeed, we can check in Appendix B that $\hat{\Gamma}_\sigma, \hat{\Gamma}_{\sigma'}$ on the same link satisfies the KL condition,

$$\hat{P}_{\text{inv}} \hat{\Gamma}_\sigma^\dagger \hat{\Gamma}_{\sigma'} \hat{P}_{\text{inv}} = \delta_{\sigma,\sigma'} \hat{P}_{\text{inv}}, \quad (29)$$

Thus $\hat{\Gamma}_\sigma$ -type errors are correctable. Another way to obtain the conclusion is through the code distance d_{code} : for a QEC with code distance d_{code} , errors involving up to $[(d_{\text{code}} - 1)/2]$ qudits are guaranteed to be correctable [110]. In our case, to make a logical error with $\hat{\Gamma}_\sigma$ -type operators, one needs at least four links of a plaquette to form a Wilson loop, thus the code distance is 4. This makes any $[(4 - 1)/2] = 1$ $\hat{\Gamma}_\sigma$ -type error correctable.

The errors induced by the $\hat{L}_g(\mathbf{x}, i)$ operator are not detectable if g is the Abelian center of the group as it commutes with the \hat{P}_{inv} . For g not in the Abelian center, if $\hat{L}_g(\mathbf{x}, i)$ drifts a state to another gauge invariant state, we can not detect such errors. On the other hand when the error $\hat{L}_g(\mathbf{x}, i)$ drifts a state out of the invariant

² We will reserve the terms “physical states (space)” for the gauge-symmetric ones in the LGT which is unfortunately different from the convention of the QEC literature. Terms “physical qubits (qudits, noise)” still refer to any qubits (qudits, noise) in $\mathcal{H}_{\text{full}}$, consistent with QEC literature.

³ Γ_σ is short for $\Gamma_{\sigma,m,n}$, where σ is the irrep, and m, n indicated the matrix element in the representation. The number of different $\Gamma_{\sigma,m,n}$ is therefore $\sum_\sigma d_\sigma^2 = |G|$.

Hilbert space by generating a local charge at site \mathbf{x} , we can measure the local charge at \mathbf{x} and detect such errors. However, as $\hat{L}_g(\mathbf{x}, i)$ does not affect local charges at other sites, it is not possible to diagnose the link that $\hat{L}_g(\mathbf{x}, i)$ affects, and thus the errors are not correctable. The fact that $\hat{L}_g(\mathbf{x}, i)$ are not correctable can also be seen by checking the KL condition:

$$\hat{P}_{\text{inv}} \hat{L}_{g'}^\dagger \hat{L}_g \hat{P}_{\text{inv}} = \frac{1}{|G|} \sum_{h \in G} \hat{L}_{h^{-1}g'^{-1}gh} \hat{P}_{\text{inv}}. \quad (30)$$

The right hand side of Eq. (30) differs from Eq. (25) by an operator $\frac{1}{|G|} \sum_{h \in G} \hat{L}_{h^{-1}g'^{-1}gh}$, thus breaking the KL condition. In the Z_2 gauge theory, a Z_2 -register is a qubit, and the complete basis reduces to the familiar Pauli operators $\{I, \hat{X}, \hat{Z}, \hat{X}\hat{Z}\}$, of which $\hat{\Gamma}_\sigma \in \{I, \hat{Z}\}$ are correctable.

The correctable error set can contain multiple-link $\hat{\Gamma}_\sigma$ errors, as long as the erroneous links are separated enough such that there is no ambiguity about which link causes the gauge violation. The easiest errors to decode are those that show up as pairs of charges in dual representations $\sigma, \bar{\sigma}$ at the two ends of a link, surrounded by neighboring sites all with zero charge. This requires the $\hat{\Gamma}_\sigma$ errors to be separated by at least two error-less links (Fig. 3), which we call the *minimal effort decoding condition (MED)*. The condition can be relaxed if more complicated classical processing is available. The KL condition requires any product of two error operators \hat{N}_i and \hat{N}_j to contain no non-trivial gauge-invariant operators, i.e. Wilson loops. This condition is fulfilled when the number of links affected by Γ_σ errors along any closed loop of perimeter C is at most $\lfloor \frac{C-1}{2} \rfloor$, thus eliminating the possibility of error links in \hat{N}_i and \hat{N}_j forming loops. Considering only the smallest loops, i.e. plaquettes, the local KL condition allows at most one $\hat{\Gamma}_\sigma$ error per plaquette.

III.3. The encoding and decoding circuits

Conceptually, the encoding and decoding of gauge symmetry is easier in the electric basis, where Gauss's law reads as "zero electric flux at each vertex". For non-Abelian groups, the computation of the net flux requires the group's Clebsch-Gordan coefficients which are not diagonal in the electric basis. We bypass some of the difficulties by doing an "effective Clebsch-Gordan sum" in the group element basis. We derive in Appendix D that the Clebsch-Gordan sum is equivalent to group multiplications in the group element basis. With this, we can encode and decode Gauss's law using the following primitive gates [111] acting on group registers:

- Inverse gate: $\mathfrak{U}_{-1}|g\rangle = |g^{-1}\rangle$,
- Left and Right Multiplication gates: $\mathfrak{U}_\times^L|g\rangle|U\rangle = |g\rangle|gU\rangle$, $\mathfrak{U}_\times^R|g\rangle|U\rangle = |g\rangle|Ug\rangle$,

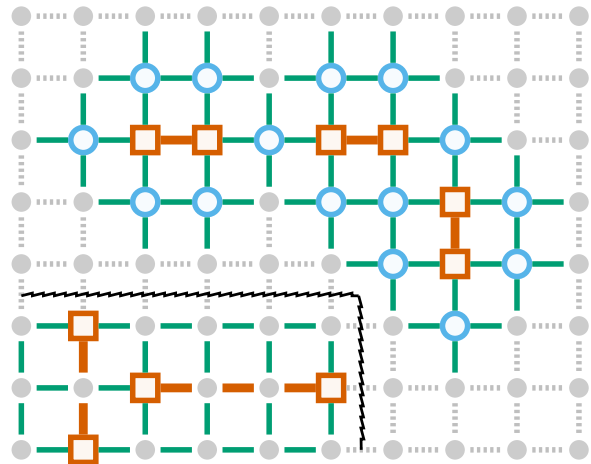


FIG. 3. Examples of correctable error distributed on the lattice to satisfy the MED (upper-right) or the local KL condition (lower-left). The orange links are Γ -type errors, which must break gauge symmetry at the orange squares. The conditions require the green links to be error-less. For the MED condition, the adjacent sites (blue circles) must be charge-neutral. For the local KL condition, the error links are allowed to extend in a straight line, which is the shortest path to connect a pair of charges.

- Fourier transform gate:

$$\mathfrak{U}_F = \sum_{g, \sigma_{mn}} \sqrt{\frac{d_\sigma}{|G|}} \Gamma_{mn}^{(\sigma)}(g) |\sigma_{mn}\rangle \langle g| \quad (31)$$

which rotates the magnetic basis to the electric one,

- Group rotation gates in irreps. This uses a group register $|U\rangle$ as the control to rotate between the vectors in the d_σ -dimensional space:

$$\begin{aligned} \mathfrak{U}_\sigma &= \sum_{U \in G} (|U\rangle \langle U|) \otimes \left(\sum_{m,n=1}^{d_\sigma} \Gamma_{mn}^{(\sigma)}(U) |n\rangle \langle m| \right) \\ &= d_\sigma^{-1/2} \sum_{m,n=1}^{d_\sigma} \hat{\Gamma}_{\sigma,m,n}^\dagger \otimes (|n\rangle \langle m|) \end{aligned} \quad (32)$$

where the second equality follows from Eq. (26). For Abelian groups, \mathfrak{U}_σ is a one-register phase gate on $|U\rangle$.

Fig. 4 shows an example of encoding and decoding for the patch of 7 gauge links connected to 2 sites in the right corner of Fig. 1. To encode, the links U_3, U_7 in the maximal tree are initialized to the color neutral state $|\mathbf{g}\rangle \equiv |G|^{-\frac{1}{2}} \sum_{g \in G} |g\rangle$, and then,

$$|U_1\rangle |U_2\rangle |\mathbf{g}\rangle |U_4\rangle \xrightarrow{\mathfrak{U}_{\text{enc}}} |G|^{-\frac{1}{2}} \sum_{g \in G} |gU_1\rangle |gU_2\rangle |g^{-1}\rangle |U_4g^{-1}\rangle \quad (33)$$

One can easily check the gauge invariance Eq. (6) for the two sites after the circuit $\mathfrak{U}_{\text{enc}}$ in Fig. 4:

$$\begin{aligned}
& \hat{T}_h |G|^{-\frac{1}{2}} \sum_{g \in G} |gU_1\rangle |gU_2\rangle |g^{-1}\rangle |U_4g^{-1}\rangle \\
& = |G|^{-\frac{1}{2}} \sum_{g' = hg \in G} |g'U_1\rangle |g'U_2\rangle |g'^{-1}\rangle |U_4g'^{-1}\rangle \quad (34)
\end{aligned}$$

In the electric basis, the circuit computes the net flux of U_1, U_2, U_4 and stores it into the tree-link U_3 , thus making the total net flux at the vertex to be zero. The same process is repeated for every vertex except \mathbf{x}_0 . Sites in the same branch of the maximal tree should be processed in sequence, from the top of the branch to the root, and different branches can be encoded in parallel.

The above procedure initializes the state to the gauge invariant one $|\Psi_{\text{inv}}\rangle$. During the noisy process in Fig. 2, suppose an error $\hat{\Gamma}_{\sigma,m,n}(\mathbf{x}, i)$ turns $|\Psi_{\text{inv}}\rangle$ into $\hat{\Gamma}_{\sigma,m,n}(\mathbf{x}, i) |\Psi_{\text{inv}}\rangle$, creating a net flux of σ_m at \mathbf{x} and $\bar{\sigma}_n$ at $\mathbf{x} + \mathbf{i}$. We can decode this error pattern with the circuit \mathcal{U}_{dec} , which adds the electric fluxes coherently to the ancillary registers originally initialized to color neutral states. Then in the decoding (derived in Appendix C),

$$\begin{aligned}
& \hat{\Gamma}_{\sigma,m,n} |\Psi_{\text{inv}}\rangle \otimes |\mathbf{g}\rangle \otimes |\mathbf{g}\rangle \xrightarrow{\mathcal{U}_{\text{dec}}} \\
& \frac{1}{d_\sigma} \sum_{q,r} \hat{\Gamma}_{\sigma,q,r} |\Psi_{\text{inv}}\rangle \otimes |\sigma_{mq}(\mathbf{x})\rangle \otimes |\bar{\sigma}_{nr}(\mathbf{x} + \mathbf{i})\rangle. \quad (35)
\end{aligned}$$

For non-Abelian groups, \mathcal{U}_{dec} preserves the quantum numbers $\sigma, \bar{\sigma}$, but m, n can change into any integer in $[1, d_\sigma]$, and the corresponding new quantum numbers q, r are entangled with the ancillae.

To correct gauge-violating errors, the representation of the ancillary register at every site needs to be measured. This requires the quantum numbers σ, m, n in the Fourier basis to be stored in different qubits, and thus one can measure σ without collapsing m, n . Measuring $|\sigma\rangle$ in the trivial representation confirms the local gauge symmetry. Measuring any other $|\sigma\rangle$ indicates a gauge-violating error, and projects the gauge fields to a subspace orthogonal to \mathcal{H}_{inv} in $\mathcal{H}_{\text{gauge}}$. In this example, a pair of non-trivial representations $|\sigma\rangle, |\bar{\sigma}\rangle$ on the two ends of a link are measured, which indicates a $\hat{\Gamma}_\sigma$ error on the link, and the quantum numbers $|m\rangle |q\rangle, |n\rangle |r\rangle$ of the ancillae are entangled with the gauge field state. The recovery can be performed with \mathcal{U}_σ in Eq. (32):

$$\begin{aligned}
& \frac{1}{d_\sigma} \sum_{q,r} \hat{\Gamma}_{\sigma,q,r} |\Psi_{\text{inv}}\rangle \otimes (|m\rangle |q\rangle) \otimes (|n\rangle |r\rangle) \xrightarrow{\mathcal{U}_{\text{rec}}} \\
& \frac{1}{d_\sigma^{3/2}} \sum_{q,k,r} \hat{\Gamma}_{\sigma,q,k}^\dagger \hat{\Gamma}_{\sigma,q,r} |\Psi_{\text{inv}}\rangle \otimes (|m\rangle |k\rangle) \otimes (|n\rangle |r\rangle) \\
& = |\Psi_{\text{inv}}\rangle \otimes \left[\frac{1}{d_\sigma^{1/2}} \sum_r (|m\rangle |r\rangle) \otimes (|n\rangle |r\rangle) \right], \quad (36)
\end{aligned}$$

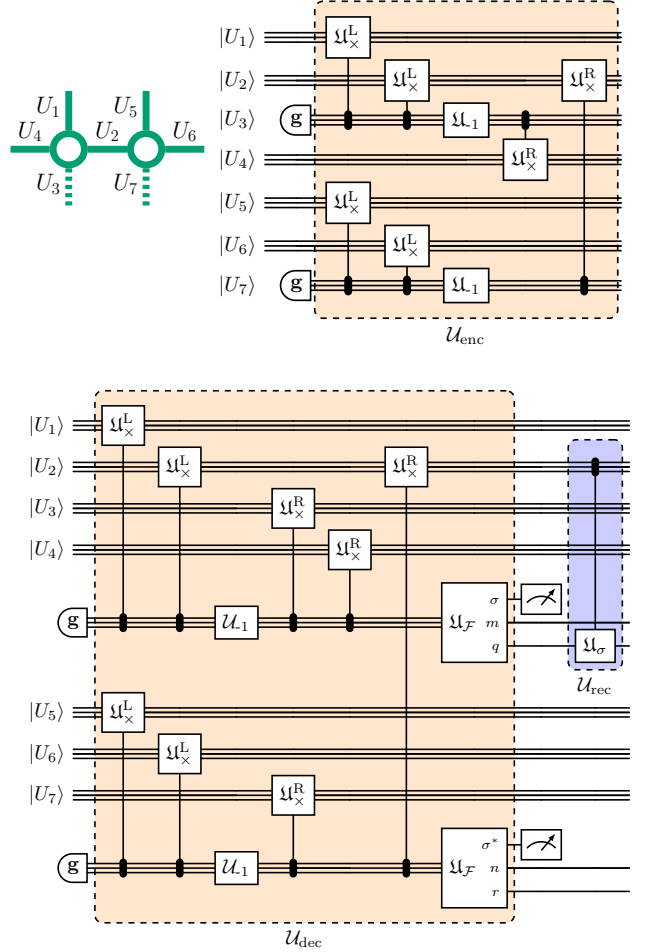


FIG. 4. Encoding and decoding circuits for the patch in Fig. 1. (top) Circuit for preparing gauge-invariant states, and (bottom) Gauss's law measurement and recovery circuit, where measuring a pair of charges $\sigma, \bar{\sigma}$ on the two ancillae indicates a gauge-violating error on $|U_2\rangle$.

where we have used the unitarity of representations,

$$d_\sigma^{-1} \sum_{q=1}^{d_\sigma} \hat{\Gamma}_{\sigma,q,k}^\dagger \hat{\Gamma}_{\sigma,q,r} = \delta_{k,r}. \quad (37)$$

Thus $|\Psi_{\text{inv}}\rangle$ is recovered and unentangled with ancillae. At this point, since the quantum information in the ancillae is irrelevant to the gauge system, one can recycle the ancillae and re-initialize them to $|\mathbf{g}\rangle$ for the next round of error detection and correction.

IV. COMPARISON OF QUANTUM FIDELITIES

IV.1. Group-agnostic thresholds

LGT states can be stored in a set of G -registers in both the gauge-fixed and gauge-redundant digitization.

The number of links needed is $N_L - N_T$ for the former and N_L for the latter. We further assume that errors on different registers are independent. Suppose the total rate for any error on a single register is ϵ . Then the quantum fidelities are lower bounded by the probability that no errors happen on any register:

$$F_{\text{fixed}} \geq (1 - \epsilon)^{N_L - N_T} \quad (38)$$

$$F_{\text{red}} \geq (1 - \epsilon)^{N_L} \quad (39)$$

With the gauge redundancy, certain configuration of $\hat{\Gamma}_\sigma$ errors are correctable via gauge symmetry checking and restoration. Suppose the correctable type error rate on a single register is ϵ_c . The lower bound for the fidelity after gauge-symmetry restoration is the probability that no error or only correctable errors happen:

$$F_{\text{restored}} \geq \sum_{n=0}^{N_L} Q_n \epsilon_c^n (1 - \epsilon)^{N_L - n} = (1 - \epsilon)^{N_L} \Xi \quad (40)$$

where Q_n is the number of ways to arrange n links with correctable errors in the lattice, such that the correctability condition is still satisfied, and Ξ is the factor by which the gauge-symmetry restoration amplifies the fidelity:

$$\Xi = \sum_{n=0}^{N_L} Q_n z^n, \quad z = \frac{\epsilon_c}{1 - \epsilon} \quad (41)$$

Comparing these two bounds Eq. (40) and Eq. (38), the condition for the gauge-symmetry restoration to give a higher fidelity than gauge fixing is

$$\Xi^{1/N_T} > (1 - \epsilon)^{-1}. \quad (42)$$

This formula can be interpreted as an error threshold: the gauge redundancy increases the code distance of Γ_σ -type errors from 1 to 4. For the fidelity to increase with the increased code distance due to gauge redundancy, ϵ has to be below certain threshold.

The Q_n 's are related to the independence polynomials of graphs (see Appendix E for details). We compute Q_n for a variety of L using the Python library `hobj` [112] up to $L = 20$ and $L = 11$ for 2d lattices with OBC and PBC, respectively, for both error-correction conditions. For 3d lattices, we are able to reach $L = 4$ for both OBC and PBC with MED condition, while only $L = 3$ for PBC with the KL condition due to limited computing resources. These Q_n are then used to compute the threshold: the ϵ where the two sides of Eq. (42) are equal at a given ϵ_c/ϵ . These are shown in black (blue) lines using OBC (PBC) in Fig. 5 and Fig. 6 for 2d and 3d lattices, respectively. Eq. (42) is satisfied in the parameter region below the lines, indicating that the gauge symmetry restoration provides higher fidelity than the gauge fixed case.

We observe two features from Fig. 5-6. First, the parameter regions to satisfy Eq. (42) only exist when $\epsilon_c/\epsilon \gtrsim 1/d$, which is consistent with the following analysis. Expanding

Eq. (42) for small ϵ , with $Q_0 = 1, Q_1 = N_L$, we have:

$$1 + \frac{N_L}{N_T} \epsilon_c + O(\epsilon_c \epsilon) > 1 + \epsilon + O(\epsilon^2). \quad (43)$$

Thus, the correctable fraction of the total error rate for a single link, ϵ_c/ϵ , must satisfy

$$\frac{\epsilon_c}{\epsilon} > \frac{N_T}{N_L} \approx \frac{1}{d}, \quad (44)$$

with $\frac{N_T}{N_L} = \frac{1}{d}$ in the infinite volume limit as seen in Tab. I. Second, in all the cases, the threshold ϵ increases as ϵ_c/ϵ increases. This is consistent with the qualitative reasoning that when a larger portion of errors are correctable, larger values of ϵ could be allowed while the redundancy still enables more correction than the errors it introduces.

Based on the error thresholds obtained at different L , we aim to extrapolate to $L \rightarrow \infty$ limit. We find that near $\epsilon = 0$, the threshold is a monotonic function of L in either boundary condition and approaches the same limit. In contrast, near $\epsilon_c/\epsilon = 1$ for 2d lattices, non-monotonic behavior is observed for small lattices with $L \leq 6$ due to finite volume effects. By restricting to the results for $L > 6$ at 2d lattice, we perform both quadratic and exponential extrapolations to obtain the threshold ϵ in the $L \rightarrow \infty$ limit which can be found in Fig. 5 (red line with the thickness quantifying error bar on extrapolations). For 3d lattice, as computing resources limit the calculations to only $L < 5$, the extrapolation to $L \rightarrow \infty$ cannot be reliably performed. For MED condition, the threshold curve with OBC near $\epsilon_c/\epsilon = 1$ exhibits a larger deviation from the PBC results at larger L , suggesting that $L < 5$ is far from the infinite limit. For the KL condition, calculations are limited to only $L = 2, 3$ with PBC, also precluding an extrapolation to infinity limit. Despite this, we expect the thresholds for $L \rightarrow \infty$ to be roughly bounded by the largest L results for OBC and PBC.

IV.2. ϵ, ϵ_c from error models

\hat{N}_j on a G -register can always be decomposed as

$$\hat{N}_j = \sum_{g,\sigma} c_{j,g,\sigma} \hat{L}_g \hat{\Gamma}_\sigma. \quad (45)$$

The trace-preserving feature $\sum_j \hat{N}_j^\dagger \hat{N}_j = \mathbb{1}$ requires $\sum_{j,\sigma,g} |c_{j,g,\sigma}|^2 = 1$. When the noise channel is diagonal in this basis, i.e. for each \hat{N}_j there is only one non-zero $c_{j,g,\sigma}$, such that we can relabel $c_{j,g,\sigma}$ to $c_{g,\sigma}$. The one-register noise channel can be written as

$$\mathcal{N}(\rho) = \sum_{g,\sigma} |c_{g,\sigma}|^2 \hat{L}_g \hat{\Gamma}_\sigma \rho (\hat{L}_g \hat{\Gamma}_\sigma)^\dagger. \quad (46)$$

The one register total error probability is

$$\epsilon = \sum_{g \neq \mathbb{1}, \sigma \neq \mathbb{1}} |c_{g,\sigma}|^2 = 1 - |c_{\mathbb{1},\mathbb{1}}|^2. \quad (47)$$

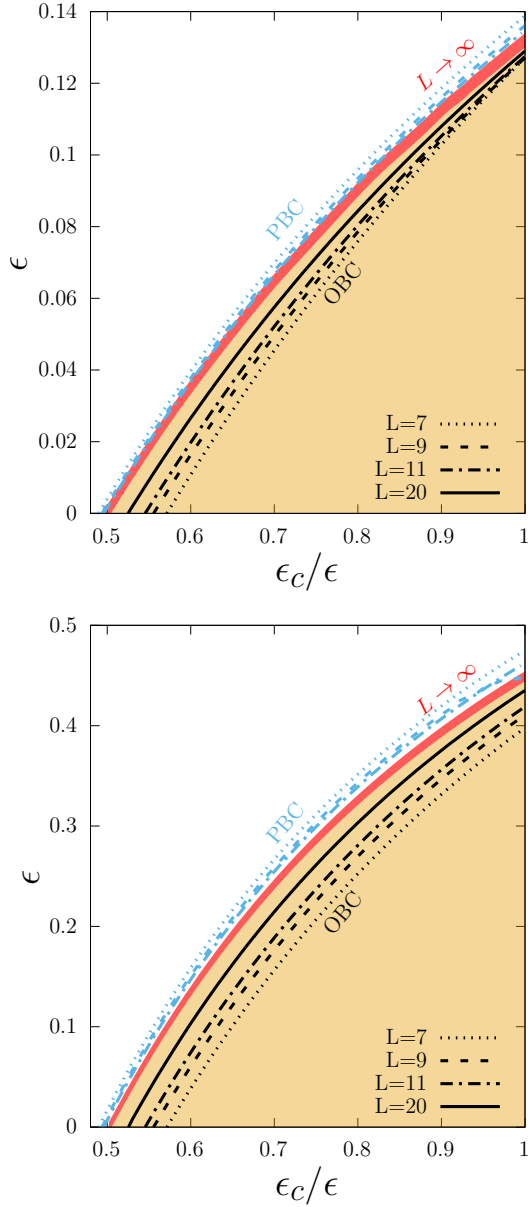


FIG. 5. Error threshold lines in the $\epsilon - \epsilon_c/\epsilon$ plane below which $F_{\text{restored}} > F_{\text{fixed}}$, indicating that using gauge redundancy to detect and correct the errors is advantageous, for 2d lattices for (top) MED condition and (bottom) local KL condition. The shaded region is the infinite volume limit.

where $g \neq \mathbb{1}$ and $\sigma \neq \mathbb{1}$ mean, respectively, that the group element cannot be the identity, and the irreducible representation cannot be the trivial one. With this, the correctable error probability is

$$\epsilon_c = \sum_{\sigma \neq \mathbb{1}} |c_{\mathbb{1},\sigma}|^2 \quad (48)$$

We consider Z_N theory, where each G -register is a qudit with N states [76]. We represent the computational basis of the qudit as $|n\rangle$, where n is an integer in $[0, N-1]$. In

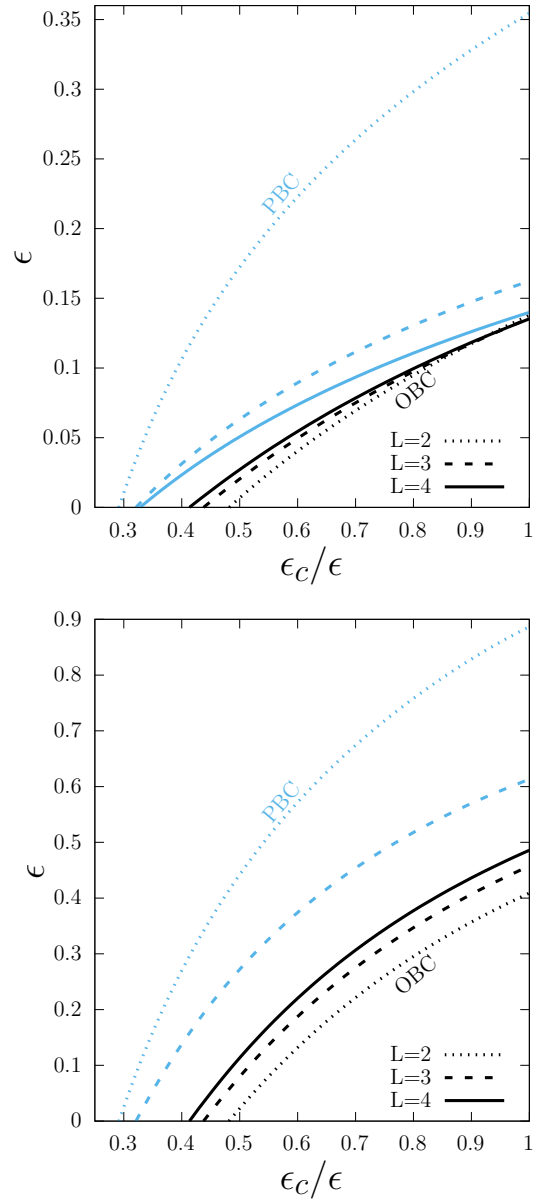


FIG. 6. Error threshold lines in the $\epsilon - \epsilon_c/\epsilon$ plane below which $F_{\text{restored}} > F_{\text{fixed}}$, indicating that using gauge redundancy to detect and correct the errors is advantageous, for 3d lattices for (top) MED condition and (bottom) local KL condition.

the computational basis, define the clock shift operators

$$\hat{\chi} = \sum_{n=0}^{N-1} |n\rangle \langle (n+1) \bmod N| \quad (49)$$

and the phase shift operators

$$\hat{\nu} = \sum_{n=0}^{N-1} e^{2\pi i n/N} |n\rangle \langle n|. \quad (50)$$

For the group Z_N , both group elements g and group representations σ can be mapped to integers $[0, N-1]$.

Thus we can choose to have the computational basis as either the group element or the electric basis. If we choose the group element basis, \hat{L}_g are clock shifts

$$\hat{L}_g = (\hat{\chi})^g = \sum_{n=0}^{N-1} |n\rangle \langle (n+g) \bmod N|, \quad (51)$$

which preserves the gauge symmetry, and thus cannot be diagnosed by Gauss's law. The representation $\hat{\Gamma}_\sigma$ operators are phase shifts

$$\hat{\Gamma}_\sigma = (\hat{\nu})^\sigma = \sum_{n=0}^{N-1} e^{2\pi i n \sigma / N} |n\rangle \langle n|. \quad (52)$$

They break gauge symmetry unless they form closed Wilson loops.

If we choose the electric basis as the computational basis instead, as the phase shift is mapped to the \hat{L}_g operator as $\hat{L}_g = (\hat{\nu})^g$, thus the phase shift errors would preserve the symmetry. While the clock shift is mapped to $\hat{\Gamma}_\sigma$ as $\hat{\Gamma}_\sigma = (\hat{\chi})^\sigma$, making the clock shift errors correctable.

Consider the error channel where single clock and phase shifts occur independently with probabilities p_χ, p_ν :

$$\begin{aligned} \mathcal{N}(\rho) = & (1 - p_\chi)(1 - p_\nu)\rho \\ & + \frac{(1 - p_\chi)p_\nu}{N-1} \sum_{i=1}^{N-1} (\hat{\nu})^i \rho (\hat{\nu})^{i\dagger} \\ & + \frac{(1 - p_\nu)p_\chi}{N-1} \sum_{j=1}^{N-1} (\hat{\chi})^j \rho (\hat{\chi})^{j\dagger} \\ & + \frac{p_\nu p_\chi}{(N-1)^2} \sum_{i,j=1}^{N-1} (\hat{\nu})^i (\hat{\chi})^j \rho (\hat{\chi})^{j\dagger} (\hat{\nu})^{i\dagger} \end{aligned} \quad (53)$$

The one register total error probability is

$$\epsilon = 1 - (1 - p_\chi)(1 - p_\nu) \quad (54)$$

In the group element basis, $(\hat{\nu})^\sigma$ are correctable, and thus

$$\epsilon_c = (1 - p_\chi)p_\nu. \quad (55)$$

In the electric basis, $(\hat{\chi})^\sigma$ are correctable,

$$\epsilon_c = (1 - p_\nu)p_\chi. \quad (56)$$

From this, we observe that the relative error probabilities of physical hardware can prefer different encodings. If the phase errors are more frequent than the clock errors ($p_\nu > p_\chi$), encoding in the group element basis will help to stay below the error thresholds with the total ϵ reasonably small.

The correctability of phase errors can be generalized to non-Abelian groups, if one chooses the group element basis encoding. This is because all operators diagonal in the group element basis can be written as linear combinations of $\hat{\Gamma}_\sigma$. For example, in Tab. II, we list the correctable

1-d representations		2-d representation	
$\hat{\Gamma}_{\text{triv}}$	\hat{I}	$\hat{\Gamma}_{2,1,1}$	$\hat{Z}_a \hat{Z}_b^{1/2} \frac{1+\hat{Z}_c}{2}$
$\hat{\Gamma}_{i\text{-ker}}$	\hat{Z}_c	$\hat{\Gamma}_{2,1,2}$	$\hat{Z}_a \hat{Z}_b^{1/2} \frac{1-\hat{Z}_c}{2}$
$\hat{\Gamma}_{j\text{-ker}}$	\hat{Z}_b	$\hat{\Gamma}_{2,2,1}$	$-\hat{Z}_a \hat{Z}_b^{3/2} \frac{1-\hat{Z}_c}{2}$
$\hat{\Gamma}_{k\text{-ker}}$	$\hat{Z}_b \hat{Z}_c$	$\hat{\Gamma}_{2,2,2}$	$\hat{Z}_a \hat{Z}_b^{3/2} \frac{1+\hat{Z}_c}{2}$

TABLE II. Correctable errors $\hat{\Gamma}_\sigma$ for the quaternion group \mathbb{Q}_8 encoded in 3 qubits via $(-1)^a i^b j^c \rightarrow |abc\rangle$.

errors for the 3-qubit encoding of the quaternion group $\mathbb{Q}_8 = \{(-1)^a i^b j^c\}$, where $a, b, c = 0$ or 1 [76]. It has four 1d representations and one 2d representation. All the Pauli-Z operators are correctable, as \hat{Z}_b, \hat{Z}_c correspond to two 1-d representation operators, and \hat{Z}_a is a linear combination of 2-d representation operators:

$$\hat{Z}_a = \frac{1}{1+i} (\hat{\Gamma}_{2,1,1} + \hat{\Gamma}_{2,1,2} - i\hat{\Gamma}_{2,2,1} + i\hat{\Gamma}_{2,2,2}). \quad (57)$$

Thus, for the error model that allows one of the three qubits to have a Pauli error,

$$\begin{aligned} \mathcal{N}(\rho) = & (1 - 3p_X - 3p_Y - 3p_Z)\rho + p_X \sum_{i=a,b,c} \hat{X}_i \rho \hat{X}_i \\ & + p_Y \sum_{i=a,b,c} \hat{Y}_i \rho \hat{Y}_i + p_Z \sum_{i=a,b,c} \hat{Z}_i \rho \hat{Z}_i \end{aligned} \quad (58)$$

with the one-register error rate being $3(p_X + p_Y + p_Z)$, the correctable fraction is

$$\frac{\epsilon_c}{\epsilon} = \frac{p_Z}{p_X + p_Y + p_Z}. \quad (59)$$

If the qubits have more phase errors and fewer bit-flip errors, encoding in the group element basis is preferable.

V. CONCLUSIONS

In this work, we explore how the natural gauge redundancy of lattice gauge theories can become a tool to create partial error correction codes for quantum simulations. For generic groups, treating the gauge transformations in lattice gauge theories as stabilizers and the gauge-invariant subspace as the code space, we identify the correctable errors in one lattice link, as well as the MED and KL conditions for multiple link errors to remain correctable. We construct the quantum circuits to prepare gauge invariant states including redundant degrees of freedoms, as well as to detect and recover the correctable errors.

We calculate the error-rate thresholds below which keeping gauge redundancy is preferable to gauge fixing for error-correcting purposes, under both the MED and KL conditions. We do this by comparing the quantum fidelities when errors exist, which is the probability that either no error happens or only correctable errors happen. The thresholds depend on the correctable fraction of the

error rate in a single link, ϵ_c/ϵ . We find a simple analytic relation at leading order in ϵ for when gauge redundancy is advantageous: $\epsilon_c/\epsilon \geq 1/d$ for a d dimensional lattice. Numerical results demonstrate that this relation is robust for realistic error rates. Thus for quantum devices where error correction is possible, $\epsilon \ll 1$, our results can be a guidance to design digitizations. To provide examples of how one may apply such thresholds, we obtain ϵ_c/ϵ explicitly for the discrete Abelian group \mathbb{Z}_N and the non-Abelian group \mathbb{Q}_8 assuming certain reasonable error models.

Consideration of similar error thresholds should be generalized to other digitization schemes and error models. The quantitative values of the thresholds found in this paper can vary depending on the computational tasks and the hardware. Future research directions should also

take into account non-diagonal error channels, quantum architectures and inclusion of fermions on the lattice sites.

ACKNOWLEDGMENTS

The authors thank Mario Pernici for his invaluable assistance with `hobj`. This work is supported by the Department of Energy through the Fermilab QuantISED program in the area of “Intersections of QIS and Theoretical Particle Physics”. Fermilab is operated by Fermi Research Alliance, LLC under contract number DE-AC02-07CH11359 with the United States Department of Energy. Y.-Y. L is supported by the NSF of China through Grant No. 12305107, 12247103.

-
- [1] A. Polkovnikov and V. Gritsev, Breakdown of the adiabatic limit in low-dimensional gapless systems, *Nature Physics* **4**, 477 (2008).
- [2] S. Baum, M. Carena, N. R. Shah, C. E. M. Wagner, and Y. Wang, Nucleation is more than critical: A case study of the electroweak phase transition in the NMSSM, *JHEP* **03**, 055, [arXiv:2009.10743 \[hep-ph\]](#).
- [3] A. Riera, C. Gogolin, and J. Eisert, Thermalization in nature and on a quantum computer, *Phys. Rev. Lett.* **108**, 080402 (2012).
- [4] A. M. Czajka, Z.-B. Kang, H. Ma, and F. Zhao, Quantum simulation of chiral phase transitions, *JHEP* **08**, 209, [arXiv:2112.03944 \[hep-ph\]](#).
- [5] T. D. Cohen, H. Lamm, S. Lawrence, and Y. Yamauchi (NuQS), Quantum algorithms for transport coefficients in gauge theories, *Phys. Rev. D* **104**, 094514 (2021), [arXiv:2104.02024 \[hep-lat\]](#).
- [6] H. Lamm, S. Lawrence, and Y. Yamauchi (NuQS), Parton physics on a quantum computer, *Phys. Rev. Res.* **2**, 013272 (2020), [arXiv:1908.10439 \[hep-lat\]](#).
- [7] M. Kreshchuk, W. M. Kirby, G. Goldstein, H. Beauchemin, and P. J. Love, Quantum Simulation of Quantum Field Theory in the Light-Front Formulation (2020), [arXiv:2002.04016 \[quant-ph\]](#).
- [8] M. Echevarria, I. Egusquiza, E. Rico, and G. Schnell, Quantum Simulation of Light-Front Parton Correlators (2020), [arXiv:2011.01275 \[quant-ph\]](#).
- [9] C. W. Bauer, M. Freytsis, and B. Nachman, Simulating Collider Physics on Quantum Computers Using Effective Field Theories, *Phys. Rev. Lett.* **127**, 212001 (2021), [arXiv:2102.05044 \[hep-ph\]](#).
- [10] T. Li, X. Guo, W. K. Lai, X. Liu, E. Wang, H. Xing, D.-B. Zhang, and S.-L. Zhu (QuNu), Partonic collinear structure by quantum computing, *Phys. Rev. D* **105**, L111502 (2022), [arXiv:2106.03865 \[hep-ph\]](#).
- [11] T. V. Zache, D. González-Cuadra, and P. Zoller, Fermion-qudit quantum processors for simulating lattice gauge theories with matter (2023), [arXiv:2303.08683 \[quant-ph\]](#).
- [12] R. P. Feynman, Simulating physics with computers, *Int. J. Theor. Phys.* **21**, 467 (1982).
- [13] S. P. Jordan, H. Krovi, K. S. Lee, and J. Preskill, BQP-completeness of Scattering in Scalar Quantum Field Theory, *Quantum* **2**, 44 (2018), [arXiv:1703.00454 \[quant-ph\]](#).
- [14] M. C. Bañuls *et al.*, Simulating Lattice Gauge Theories within Quantum Technologies, *Eur. Phys. J. D* **74**, 165 (2020), [arXiv:1911.00003 \[quant-ph\]](#).
- [15] C. W. Bauer *et al.*, Quantum Simulation for High-Energy Physics, *PRX Quantum* **4**, 027001 (2023), [arXiv:2204.03381 \[quant-ph\]](#).
- [16] A. F. Shaw, P. Lougovski, J. R. Stryker, and N. Wiebe, Quantum Algorithms for Simulating the Lattice Schwinger Model, *Quantum* **4**, 306 (2020), [arXiv:2002.11146 \[quant-ph\]](#).
- [17] Y. Tong, V. V. Albert, J. R. McClean, J. Preskill, and Y. Su, Provably accurate simulation of gauge theories and bosonic systems, *Quantum* **6**, 816 (2022), [arXiv:2110.06942 \[quant-ph\]](#).
- [18] Y. Ji, H. Lamm, and S. Zhu (NuQS), Gluon Field Digitization via Group Space Decimation for Quantum Computers, *Phys. Rev. D* **102**, 114513 (2020), [arXiv:2005.14221 \[hep-lat\]](#).
- [19] M. Carena, E. J. Gustafson, H. Lamm, Y.-Y. Li, and W. Liu, Gauge theory couplings on anisotropic lattices, *Phys. Rev. D* **106**, 114504 (2022).
- [20] C. W. Bauer, I. D’Andrea, M. Freytsis, and D. M. Grabowska, A new basis for Hamiltonian SU(2) simulations (2023), [arXiv:2307.11829 \[hep-ph\]](#).
- [21] A. N. Ciavarella, Quantum Simulation of Lattice QCD with Improved Hamiltonians (2023), [arXiv:2307.05593 \[hep-lat\]](#).
- [22] M. Hanada, J. Liu, E. Rinaldi, and M. Tezuka, Estimating truncation effects of quantum bosonic systems using sampling algorithms (2022), [arXiv:2212.08546 \[quant-ph\]](#).
- [23] E. Zohar and M. Burrello, Formulation of lattice gauge theories for quantum simulations, *Phys. Rev.* **D91**, 054506 (2015), [arXiv:1409.3085 \[quant-ph\]](#).
- [24] E. Zohar, A. Farace, B. Reznik, and J. I. Cirac, Digital lattice gauge theories, *Phys. Rev.* **A95**, 023604 (2017), [arXiv:1607.08121 \[quant-ph\]](#).
- [25] J. Bender, E. Zohar, A. Farace, and J. I. Cirac, Digital quantum simulation of lattice gauge theories in three

- spatial dimensions, *New J. Phys.* **20**, 093001 (2018), [arXiv:1804.02082 \[quant-ph\]](#).
- [26] E. J. Gustafson, H. Lamm, F. Lovelace, and D. Musk, Primitive quantum gates for an $SU(2)$ discrete subgroup: Binary tetrahedral, *Phys. Rev. D* **106**, 114501 (2022), [arXiv:2208.12309 \[quant-ph\]](#).
- [27] D. C. Hackett, K. Howe, C. Hughes, W. Jay, E. T. Neil, and J. N. Simone, Digitizing Gauge Fields: Lattice Monte Carlo Results for Future Quantum Computers, *Phys. Rev. A* **99**, 062341 (2019), [arXiv:1811.03629 \[quant-ph\]](#).
- [28] T. Hartung, T. Jakobs, K. Jansen, J. Ostmeier, and C. Urbach, Digitising $SU(2)$ gauge fields and the freezing transition, *Eur. Phys. J. C* **82**, 237 (2022), [arXiv:2201.09625 \[hep-lat\]](#).
- [29] T. Jakobs, M. Garofalo, T. Hartung, K. Jansen, J. Ostmeier, D. Rolfes, S. Romiti, and C. Urbach, Canonical Momenta in Digitized $SU(2)$ Lattice Gauge Theory: Definition and Free Theory (2023), [arXiv:2304.02322 \[hep-lat\]](#).
- [30] C. Charles, E. J. Gustafson, E. Hardt, F. Herren, N. Hogan, H. Lamm, S. Starecheski, R. S. Van de Water, and M. L. Wagman, Simulating \mathbb{Z}_2 lattice gauge theory on a quantum computer (2023), [arXiv:2305.02361 \[hep-lat\]](#).
- [31] E. J. Gustafson, H. Lamm, and F. Lovelace, Primitive Quantum Gates for an $SU(2)$ Discrete Subgroup: Binary Octahedral (2023), [arXiv:2312.10285 \[hep-lat\]](#).
- [32] E. Zohar, J. I. Cirac, and B. Reznik, Cold-Atom Quantum Simulator for $SU(2)$ Yang-Mills Lattice Gauge Theory, *Phys. Rev. Lett.* **110**, 125304 (2013), [arXiv:1211.2241 \[quant-ph\]](#).
- [33] E. Zohar, J. I. Cirac, and B. Reznik, Simulating Compact Quantum Electrodynamics with ultracold atoms: Probing confinement and nonperturbative effects, *Phys. Rev. Lett.* **109**, 125302 (2012), [arXiv:1204.6574 \[quant-ph\]](#).
- [34] E. Zohar, J. I. Cirac, and B. Reznik, Quantum Simulations of Lattice Gauge Theories using Ultracold Atoms in Optical Lattices, *Rept. Prog. Phys.* **79**, 014401 (2016), [arXiv:1503.02312 \[quant-ph\]](#).
- [35] H. Singh and S. Chandrasekharan, Qubit regularization of the $O(3)$ sigma model, *Phys. Rev. D* **100**, 054505 (2019), [arXiv:1905.13204 \[hep-lat\]](#).
- [36] H. Singh, Qubit $O(N)$ nonlinear sigma models (2019), [arXiv:1911.12353 \[hep-lat\]](#).
- [37] A. J. Buser, T. Bhattacharya, L. Cincio, and R. Gupta, Quantum simulation of the qubit-regularized $O(3)$ -sigma model (2020), [arXiv:2006.15746 \[quant-ph\]](#).
- [38] J. F. Haase, L. Dellantonio, A. Celi, D. Paulson, A. Kan, K. Jansen, and C. A. Muschik, A resource efficient approach for quantum and classical simulations of gauge theories in particle physics (2020), [arXiv:2006.14160 \[quant-ph\]](#).
- [39] A. Alexandru, P. F. Bedaque, A. Carosso, M. J. Cervia, and A. Sheng, Qubitization strategies for bosonic field theories, *Phys. Rev. D* **107**, 034503 (2023), [arXiv:2209.00098 \[hep-lat\]](#).
- [40] A. Alexandru, P. F. Bedaque, A. Carosso, M. J. Cervia, E. M. Murairi, and A. Sheng, Fuzzy Gauge Theory for Quantum Computers (2023), [arXiv:2308.05253 \[hep-lat\]](#).
- [41] U.-J. Wiese, Towards Quantum Simulating QCD, *Proceedings, 24th International Conference on Ultra-Relativistic Nucleus-Nucleus Collisions (Quark Matter 2014): Darmstadt, Germany, May 19-24, 2014*, *Nucl. Phys.* **A931**, 246 (2014), [arXiv:1409.7414 \[hep-th\]](#).
- [42] D. Luo, J. Shen, M. Highman, B. K. Clark, B. DeMarco, A. X. El-Khadra, and B. Gadway, A Framework for Simulating Gauge Theories with Dipolar Spin Systems (2019), [arXiv:1912.11488 \[quant-ph\]](#).
- [43] R. C. Brower, D. Berenstein, and H. Kawai, Lattice Gauge Theory for a Quantum Computer, *PoS LATTICE2019*, 112 (2019), [arXiv:2002.10028 \[hep-lat\]](#).
- [44] S. V. Mathis, G. Mazzola, and I. Tavernelli, Toward scalable simulations of Lattice Gauge Theories on quantum computers, *Phys. Rev. D* **102**, 094501 (2020), [arXiv:2005.10271 \[quant-ph\]](#).
- [45] E. Zohar, J. I. Cirac, and B. Reznik, Quantum simulations of gauge theories with ultracold atoms: local gauge invariance from angular momentum conservation, *Phys. Rev. A* **88**, 023617 (2013), [arXiv:1303.5040 \[quant-ph\]](#).
- [46] D. B. Kaplan and J. R. Stryker, Gauss's law, duality, and the hamiltonian formulation of $u(1)$ lattice gauge theory, *Phys. Rev. D* **102**, 094515 (2020).
- [47] J. Bender and E. Zohar, Gauge redundancy-free formulation of compact qed with dynamical matter for quantum and classical computations, *Phys. Rev. D* **102**, 114517 (2020).
- [48] A. Yamamoto, Real-time simulation of $(2+1)$ -dimensional lattice gauge theory on qubits, *PTEP* **2021**, 013B06 (2021), [arXiv:2008.11395 \[hep-lat\]](#).
- [49] C. W. Bauer and D. M. Grabowska, Efficient Representation for Simulating $U(1)$ Gauge Theories on Digital Quantum Computers at All Values of the Coupling (2021), [arXiv:2111.08015 \[hep-ph\]](#).
- [50] D. M. Grabowska, C. Kane, B. Nachman, and C. W. Bauer, Overcoming exponential scaling with system size in Trotter-Suzuki implementations of constrained Hamiltonians: $2+1$ $U(1)$ lattice gauge theories (2022), [arXiv:2208.03333 \[quant-ph\]](#).
- [51] C. Kane, D. M. Grabowska, B. Nachman, and C. W. Bauer, Efficient quantum implementation of $2+1$ $U(1)$ lattice gauge theories with Gauss law constraints (2022), [arXiv:2211.10497 \[quant-ph\]](#).
- [52] D. Paulson, L. Dellantonio, J. F. Haase, A. Celi, A. Kan, A. Jena, C. Kokail, R. van Bijnen, K. Jansen, P. Zoller, and C. A. Muschik, Simulating 2d effects in lattice gauge theories on a quantum computer, *PRX Quantum* **2**, 030334 (2021).
- [53] M. Kreshchuk, S. Jia, W. M. Kirby, G. Goldstein, J. P. Vary, and P. J. Love, Light-Front Field Theory on Current Quantum Computers (2020), [arXiv:2009.07885 \[quant-ph\]](#).
- [54] N. Klco, J. R. Stryker, and M. J. Savage, $SU(2)$ non-Abelian gauge field theory in one dimension on digital quantum computers, *Phys. Rev. D* **101**, 074512 (2020), [arXiv:1908.06935 \[quant-ph\]](#).
- [55] A. Ciavarella, N. Klco, and M. J. Savage, A Trailhead for Quantum Simulation of $SU(3)$ Yang-Mills Lattice Gauge Theory in the Local Multiplet Basis (2021), [arXiv:2101.10227 \[quant-ph\]](#).
- [56] T. V. Zache, D. González-Cuadra, and P. Zoller, Quantum and classical spin network algorithms for q -deformed Kogut-Susskind gauge theories (2023), [arXiv:2304.02527 \[quant-ph\]](#).
- [57] T. Hayata and Y. Hidaka, Breaking new ground for quantum and classical simulations of $SU(3)$ Yang-Mills theory (2023), [arXiv:2306.12324 \[hep-lat\]](#).
- [58] E. Zohar and B. Reznik, Confinement and lattice QED

- electric flux-tubes simulated with ultracold atoms, *Phys. Rev. Lett.* **107**, 275301 (2011), [arXiv:1108.1562 \[quant-ph\]](#).
- [59] D. Banerjee, M. Bögli, M. Dalmonte, E. Rico, P. Stebler, U. J. Wiese, and P. Zoller, Atomic Quantum Simulation of $U(N)$ and $SU(N)$ Non-Abelian Lattice Gauge Theories, *Phys. Rev. Lett.* **110**, 125303 (2013), [arXiv:1211.2242 \[cond-mat.quant-gas\]](#).
- [60] L. Tagliacozzo, A. Celi, P. Orland, and M. Lewenstein, Simulations of non-Abelian gauge theories with optical lattices, *Nature Commun.* **4**, 2615 (2013).
- [61] I. Raychowdhury and J. R. Stryker, Solving gauss's law on digital quantum computers with loop-string-hadron digitization, *Phys. Rev. Res.* **2**, 033039 (2020).
- [62] F. M. Surace, P. P. Mazza, G. Giudici, A. Lerose, A. Gambassi, and M. Dalmonte, Lattice gauge theories and string dynamics in Rydberg atom quantum simulators, *Phys. Rev. X* **10**, 021041 (2020).
- [63] Z. Davoudi, I. Raychowdhury, and A. Shaw, Search for Efficient Formulations for Hamiltonian Simulation of non-Abelian Lattice Gauge Theories (2020), [arXiv:2009.11802 \[hep-lat\]](#).
- [64] T. Bhattacharya, A. J. Buser, S. Chandrasekharan, R. Gupta, and H. Singh, Qubit regularization of asymptotic freedom (2020), [arXiv:2012.02153 \[hep-lat\]](#).
- [65] J. Zhou, H. Singh, T. Bhattacharya, S. Chandrasekharan, and R. Gupta, Spacetime symmetric qubit regularization of the asymptotically free two-dimensional $O(4)$ model, *Phys. Rev. D* **105**, 054510 (2022).
- [66] S. Caspar and H. Singh, From Asymptotic Freedom to θ Vacua: Qubit Embeddings of the $O(3)$ Nonlinear σ Model, *Phys. Rev. Lett.* **129**, 022003 (2022), [arXiv:2203.15766 \[hep-lat\]](#).
- [67] J. R. Stryker, Oracles for Gauss's law on digital quantum computers, *Phys. Rev.* **A99**, 042301 (2019), [arXiv:1812.01617 \[quant-ph\]](#).
- [68] H. Lamm, S. Lawrence, and Y. Yamauchi (NuQS), Suppressing Coherent Gauge Drift in Quantum Simulations (2020), [arXiv:2005.12688 \[quant-ph\]](#).
- [69] E. Mathew and I. Raychowdhury, Protecting local and global symmetries in simulating (1+1)D non-Abelian gauge theories, *Phys. Rev. D* **106**, 054510 (2022), [arXiv:2206.07444 \[hep-lat\]](#).
- [70] M. Van Damme, J. Mildenberger, F. Grusdt, P. Hauke, and J. C. Halimeh, Suppressing nonperturbative gauge errors in the thermodynamic limit using local pseudo-generators (2021), [arXiv:2110.08041 \[quant-ph\]](#).
- [71] J. C. Halimeh and P. Hauke, Stabilizing Gauge Theories in Quantum Simulators: A Brief Review (2022) [arXiv:2204.13709 \[cond-mat.quant-gas\]](#).
- [72] S. Lieu, R. Belyansky, J. T. Young, R. Lundgren, V. V. Albert, and A. V. Gorshkov, Symmetry breaking and error correction in open quantum systems, *Phys. Rev. Lett.* **125**, 240405 (2020).
- [73] M. Van Damme, J. C. Halimeh, and P. Hauke, Gauge-Symmetry Violation Quantum Phase Transition in Lattice Gauge Theories (2020), [arXiv:2010.07338 \[cond-mat.quant-gas\]](#).
- [74] C. Bonati, A. Pelissetto, and E. Vicari, Breaking of Gauge Symmetry in Lattice Gauge Theories, *Phys. Rev. Lett.* **127**, 091601 (2021).
- [75] C. Bonati, A. Pelissetto, and E. Vicari, Lattice gauge theories in the presence of a linear gauge-symmetry breaking, *Phys. Rev. E* **104**, 014140 (2021).
- [76] E. J. Gustafson and H. Lamm, Robustness of Gauge Digitization to Quantum Noise (2023), [arXiv:2301.10207 \[hep-lat\]](#).
- [77] K. Stannigel, P. Hauke, D. Marcos, M. Hafezi, S. Diehl, M. Dalmonte, and P. Zoller, Constrained dynamics via the Zeno effect in quantum simulation: Implementing non-Abelian lattice gauge theories with cold atoms, *Phys. Rev. Lett.* **112**, 120406 (2014).
- [78] J. C. Halimeh, H. Lang, J. Mildenberger, Z. Jiang, and P. Hauke, Gauge-Symmetry Protection Using Single-Body Terms (2020), [arXiv:2007.00668 \[quant-ph\]](#).
- [79] J. C. Halimeh, R. Ott, I. P. McCulloch, B. Yang, and P. Hauke, Robustness of gauge-invariant dynamics against defects in ultracold-atom gauge theories, *Phys. Rev. Res.* **2**, 033361 (2020), [arXiv:2005.10249 \[cond-mat.quant-gas\]](#).
- [80] J. C. Halimeh, H. Lang, and P. Hauke, Gauge protection in non-Abelian lattice gauge theories (2021), [arXiv:2106.09032 \[cond-mat.quant-gas\]](#).
- [81] M. C. Tran, Y. Su, D. Carney, and J. M. Taylor, Faster digital quantum simulation by symmetry protection, *PRX Quantum* **2**, 010323 (2021).
- [82] A. Rajput, A. Roggero, and N. Wiebe, Quantum error correction with gauge symmetries, *npj Quantum Information* **9**, 41 (2023).
- [83] B. M. Terhal, Quantum error correction for quantum memories, *Rev. Mod. Phys.* **87**, 307 (2015).
- [84] J. Roffe, Quantum error correction: an introductory guide, *Contemporary Physics* **60**, 226 (2019).
- [85] [Scaling IonQ's quantum computers: The roadmap \(2020\)](#).
- [86] [The IBM Quantum Development Roadmap \(2021\)](#).
- [87] H. Neven, [Day 1 opening keynote by Hartmut Neven \(quantum summer symposium 2020\) \(2020\)](#).
- [88] Z. Cai, R. Babbush, S. C. Benjamin, S. Endo, W. J. Hugins, Y. Li, J. R. McClean, and T. E. O'Brien, Quantum error mitigation (2022), [arXiv:2210.00921 \[quant-ph\]](#).
- [89] N. Klco and M. J. Savage, Hierarchical qubit maps and hierarchically implemented quantum error correction, *Phys. Rev. A* **104**, 062425 (2021), [arXiv:2109.01953 \[quant-ph\]](#).
- [90] A. Rajput, A. Roggero, and N. Wiebe, Quantum error correction with gauge symmetries, *npj Quantum Inf.* **9**, 41 (2023), [arXiv:2112.05186 \[quant-ph\]](#).
- [91] J. del Pino and O. Zilberberg, Dynamical Gauge Fields with Bosonic Codes, *Phys. Rev. Lett.* **130**, 171901 (2023), [arXiv:2211.12119 \[quant-ph\]](#).
- [92] A. J. Landahl and B. C. A. Morrison, Logical fermions for fault-tolerant quantum simulation (2021), [arXiv:2110.10280 \[quant-ph\]](#).
- [93] Y.-A. Chen, A. V. Gorshkov, and Y. Xu, Error-correcting codes for fermionic quantum simulation (2022), [arXiv:2210.08411 \[quant-ph\]](#).
- [94] P. W. Shor, Fault tolerant quantum computation (1996), [arXiv:quant-ph/9605011](#).
- [95] D. Aharonov and M. Ben-Or, Fault-tolerant quantum computation with constant error rate, *SIAM Journal on Computing* **38**, 1207 (2008).
- [96] E. Knill, R. Laflamme, and W. H. Zurek, Resilient quantum computation, *Science* **279**, 342 (1998).
- [97] J. Kogut and L. Susskind, Hamiltonian formulation of Wilson's lattice gauge theories, *Phys. Rev. D* **11**, 395 (1975).
- [98] N. Bao, C. Cao, A. Chatwin-Davies, G. Cheng, and G. Zhu, Superselection rules, quantum error correction,

and quantum chromodynamics (2023), [arXiv:2306.17230 \[quant-ph\]](#).

- [99] X.-Q. Luo, S.-H. Guo, H. Kroger, and D. Schutte, Improved lattice gauge field Hamiltonian, *Phys. Rev. D* **59**, 034503 (1999), [arXiv:hep-lat/9804029](#).
- [100] J. Carlsson and B. H. McKellar, Direct improvement of Hamiltonian lattice gauge theory, *Phys. Rev. D* **64**, 094503 (2001), [arXiv:hep-lat/0105018](#).
- [101] J. Carlsson and B. H. J. McKellar, Direct improvement of hamiltonian lattice gauge theory, *Phys. Rev. D* **64**, 094503 (2001).
- [102] M. Carena, H. Lamm, Y.-Y. Li, and W. Liu, Improved hamiltonians for quantum simulations of gauge theories, *Phys. Rev. Lett.* **129**, 051601 (2022).
- [103] C. Gattringer and C. B. Lang, *Quantum chromodynamics on the lattice*, Vol. 788 (Springer, Berlin, 2010).
- [104] N. Ligterink, N. Walet, and R. Bishop, Toward a many-body treatment of hamiltonian lattice SU(n) gauge theory, *Annals of Physics* **284**, 215 (2000).
- [105] V. Müller and W. Rühl, The energy gap of su(2) lattice gauge theory in 2+1 dimensions, *Nuclear Physics B* **230**, 49 (1984).
- [106] J. B. Bronzan, Explicit hamiltonian for su(2) lattice gauge theory, *Phys. Rev. D* **31**, 2020 (1985).
- [107] Z. Cai, R. Babbush, S. C. Benjamin, S. Endo, W. J. Hugins, Y. Li, J. R. McClean, and T. E. O'Brien, Quantum error mitigation (2023), [arXiv:2210.00921 \[quant-ph\]](#).
- [108] E. Knill and R. Laflamme, Theory of quantum error-correcting codes, *Phys. Rev. A* **55**, 900 (1997).
- [109] P. M. van Den Broek and J. F. Cornwell, Clebsch-gordan coefficients of symmetry groups, *physica status solidi (b)* **90**, 211 (1978).
- [110] M. A. Nielsen and I. L. Chuang, *Quantum Computation and Quantum Information: 10th Anniversary Edition* (Cambridge University Press, 2010).
- [111] H. Lamm, S. Lawrence, and Y. Yamauchi (NuQS), General Methods for Digital Quantum Simulation of Gauge Theories, *Phys. Rev. D* **100**, 034518 (2019), [arXiv:1903.08807 \[hep-lat\]](#).
- [112] P. Butera and M. Pernici, Sums of permanental minors using Grassmann algebra (2014), [arXiv:1406.5337 \[hep-lat\]](#).

Appendix A: Counting gauge orbits

Let \mathcal{U} be the set of configurations and \mathcal{G} the group of gauge transformations on the entire lattice, with $|\mathcal{U}| = |G|^{N_L}$ and $|\mathcal{G}| = |G|^{N_V}$. In the magnetic basis, $\hat{P}_{\text{inv}}|U\rangle$ is the uniform superposition of all gauge transformations of $|U\rangle$. Thus the number of states in the basis $\hat{P}_{\text{inv}}\mathcal{U}$ is the number of configurations in \mathcal{U} that are not equivalent under gauge transformations:

$$\dim \mathcal{H}_{\text{inv}} = |\mathcal{U}/\mathcal{G}| \quad (\text{A1})$$

where $|\mathcal{U}/\mathcal{G}|$ is the number of orbits in \mathcal{U} under \mathcal{G} . According to Burnside's counting theorem,

$$|\mathcal{U}/\mathcal{G}| = \frac{1}{|\mathcal{G}|} \sum_{T \in \mathcal{G}} |\mathcal{U}^T| = \frac{1}{|\mathcal{G}|} \sum_{|U\rangle \in \mathcal{U}} |\mathcal{G}_{|U\rangle}|, \quad (\text{A2})$$

where \mathcal{U}^T is the subset of elements invariant under $T \in \mathcal{G}$,

$$\mathcal{U}^T = \{|U\rangle \in \mathcal{U} : T|U\rangle = |U\rangle\}, \quad (\text{A3})$$

and $\mathcal{G}_{|U\rangle}$ is the stabilizer group for the element $|U\rangle$,

$$\mathcal{G}_{|U\rangle} = \{T \in \mathcal{G} : T|U\rangle = |U\rangle\}. \quad (\text{A4})$$

If $T = \prod_{\mathbf{x}} \hat{T}_{h_{\mathbf{x}}}$ then with $|U\rangle = \prod_{\mathbf{x},i} |g_{\mathbf{x},i}\rangle$, there must be

$$h_{\mathbf{x}+\mathbf{i}} = g_{\mathbf{x},i}^{-1} h_{\mathbf{x}} g_{\mathbf{x},i}, \quad (\text{A5})$$

which means once $h_{\mathbf{x}_0}$ at a certain site \mathbf{x}_0 is fixed, there is at most one $T \in \mathcal{G}$ to keep $|U\rangle$ invariant. For $h_{\mathbf{x}_0} \in H$ the Abelian center of G , this is the global transformation with $h_{\mathbf{x}_0}$. Therefore $|H| \leq |\mathcal{G}_{|U\rangle}| \leq |G|$ and

$$|\mathcal{U}||H| \leq \sum_{|U\rangle \in \mathcal{U}} |\mathcal{G}_{|U\rangle}| \leq |\mathcal{U}||G|. \quad (\text{A6})$$

given that $|\mathcal{U}| = |G|^{N_L}$, $|\mathcal{G}| = |G|^{N_V}$, we find

$$|H||G|^{N_L - N_V} \leq |\mathcal{U}/\mathcal{G}| \leq |G|^{N_L - N_V + 1}. \quad (\text{A7})$$

For Abelian groups, $H = G$ and $|\mathcal{U}/\mathcal{G}| = |G|^{N_L - N_V + 1} = |G|^{N_L - N_T}$. For non-Abelian G , the “ \leq ” are both “ $<$ ”.

Appendix B: Correctability of $\hat{\Gamma}_\sigma$

In the rest of the appendices, g, h are group elements, σ, τ are irreducible representations (irreps), and $k, l, m, n, q, r, s, t, u$ are the matrix elements of representations. To check Eq. (29), we will compute in the magnetic basis

$$\hat{P}_0(\mathbf{x}) \hat{\Gamma}_{\sigma',s,q}^\dagger(\mathbf{x}, i) \hat{\Gamma}_{\sigma,m,n}(\mathbf{x}, i) \hat{P}_0(\mathbf{x}) = \frac{1}{|G|^2} \sum_{g,h \in G} \left(\begin{array}{c} \hat{L}_g \hat{L}_h \\ \hat{R}_{g^{-1}} \hat{R}_{h^{-1}} \text{---} \mathbf{x} \text{---} \hat{L}_g \hat{\Gamma}_{\sigma',s,q}^\dagger \hat{\Gamma}_{\sigma,m,n} \hat{L}_h \\ \hat{R}_{g^{-1}} \hat{R}_{h^{-1}} \end{array} \right), \quad (\text{B1})$$

For the operators on the link \mathbf{x}, i ,

$$\begin{aligned}
\hat{L}_g \hat{\Gamma}_{\sigma', s, q}^\dagger \hat{\Gamma}_{\sigma, m, n} \hat{L}_h &= \sum_U |gU\rangle \langle U| \sqrt{d_\sigma d_{\sigma'}} \Gamma_{sq}^{(\sigma')} (U) \Gamma_{mn}^{(\sigma)} (U)^* \hat{L}_h \\
&= \sqrt{d_\sigma} \left[\sum_{U, l} \Gamma_{sl}^{(\sigma')} (g^{-1}) \Gamma_{lq}^{(\sigma')} (gU) \right] \left[\sum_k \Gamma_{mk}^{(\sigma)} (g^{-1}) \Gamma_{kn}^{(\sigma)} (gU) \right]^* |gU\rangle \langle U| \hat{L}_h \\
&= \sum_{k, l} \Gamma_{sl}^{(\sigma')} (g^{-1}) \Gamma_{mk}^{(\sigma)} (g^{-1})^* \hat{\Gamma}_{\sigma', l, q}^\dagger \hat{\Gamma}_{\sigma, k, n} \hat{L}_g \hat{L}_h.
\end{aligned} \tag{B2}$$

Thus, let $h' = gh$,

$$\hat{P}_0(\mathbf{x}) \hat{\Gamma}_{\sigma', s, q}^\dagger(\mathbf{x}, i) \hat{\Gamma}_{\sigma, m, n}(\mathbf{x}, i) \hat{P}_0(\mathbf{x}) = \frac{1}{|G|^2} \sum_{h' \in G} \left(\hat{R}_{h'-1} \begin{array}{c} \hat{L}_{h'} \\ | \\ \mathbf{x} \\ | \\ \hat{R}_{h'-1} \end{array} \sum_{k, l, g} \Gamma_{sl}^{(\sigma')} (g^{-1}) \Gamma_{mk}^{(\sigma)} (g^{-1})^* \hat{\Gamma}_{\sigma', l, q}^\dagger \hat{\Gamma}_{\sigma, k, n} \hat{L}_{h'} \right). \tag{B3}$$

With the orthogonality of matrix elements

$$\sum_g \Gamma_{sl}^{(\sigma')} (g^{-1}) \Gamma_{mk}^{(\sigma)} (g^{-1})^* = \delta_{\sigma\sigma'} \delta_{ms} \delta_{lk} |G| / d_\sigma, \tag{B4}$$

and the unitarity of representations Eq. (37), we get

$$\hat{P}_0(\mathbf{x}) \hat{\Gamma}_{\sigma', s, q}^\dagger(\mathbf{x}, i) \hat{\Gamma}_{\sigma, m, n}(\mathbf{x}, i) \hat{P}_0(\mathbf{x}) = \delta_{\sigma'\sigma} \delta_{sm} \delta_{qn} \hat{P}_0(\mathbf{x}) \tag{B5}$$

Appendix C: Derivation of Eq. (35) in the group element basis

\mathcal{U}_{dec} performs the following for a gauge field state $|\Psi\rangle$:

$$\begin{aligned}
|\Psi\rangle \otimes (|G|^{-\frac{1}{2}} \sum_{g \in G} |g\rangle) &\xrightarrow{\mathfrak{U}_x^L, \mathfrak{U}_x^R, \mathfrak{U}_{-1}, \mathfrak{U}_x^L, \mathfrak{U}_x^R} |G|^{-\frac{1}{2}} \sum_{g \in G} \hat{T}_g(\mathbf{x}) |\Psi\rangle \otimes |g^{-1}\rangle \\
&\xrightarrow{QFT} \sum_{g \in G} \hat{T}_g(\mathbf{x}) |\Psi\rangle \otimes \left(\sum_{\sigma, m, n} \frac{\sqrt{d_\sigma}}{|G|} \Gamma_{mn}^{(\sigma)} (g^{-1}) |\sigma\rangle \right) = \sum_{\sigma, m, n} \hat{P}_{\sigma, mn}(\mathbf{x}) |\Psi\rangle \otimes |\sigma_{mn}\rangle,
\end{aligned} \tag{C1}$$

where

$$\hat{P}_{\sigma, mn}(\mathbf{x}) \equiv \frac{\sqrt{d_\sigma}}{|G|} \sum_{g \in G} \Gamma_{mn}^{(\sigma)} (g^{-1}) \hat{T}_g(\mathbf{x}) \tag{C2}$$

For the trivial representation $\sigma = 0$, $\hat{P}_0(\mathbf{x})$ is the projection to the subspace invariant under local gauge transformations and $\hat{P}_0(\mathbf{x}) |\Psi\rangle_{\text{inv}} = |\Psi\rangle_{\text{inv}}$. When a correctable error $\hat{\Gamma}_\sigma$ occurs on one gauge register, consider

$$\hat{P}_{\sigma'_s}(\mathbf{x}) \hat{\Gamma}_{\sigma, m, n}(\mathbf{x}, i) \hat{P}_0(\mathbf{x}) = \frac{\sqrt{d_\sigma}}{|G|^2} \sum_{g, h \in G} \Gamma_{sq}^{(\sigma')} (g^{-1}) \left(\hat{R}_{g-1} \hat{R}_{h-1} \begin{array}{c} \hat{L}_g \hat{L}_h \\ | \\ \mathbf{x} \\ | \\ \hat{R}_{g-1} \hat{R}_{h-1} \end{array} \hat{L}_g \hat{\Gamma}_{\sigma, m, n} \hat{L}_h \right), \tag{C3}$$

use the ‘‘commutation relation’’ to replace $\hat{L}_g \hat{\Gamma}_\sigma$ on the link (\mathbf{x}, i) with

$$\hat{L}_g \hat{\Gamma}_{\sigma, m, n} = \sum_U |gU\rangle \langle U| \sqrt{d_\sigma} \Gamma_{mn}^{(\sigma)} (U)^* = \sum_U |gU\rangle \langle U| \sqrt{d_\sigma} \left[\sum_k \Gamma_{mk}^{(\sigma)} (g^{-1}) \Gamma_{kn}^{(\sigma)} (gU) \right]^* = \sum_k \Gamma_{mk}^{(\sigma)} (g^{-1})^* \hat{\Gamma}_{\sigma, k, n} \hat{L}_g, \tag{C4}$$

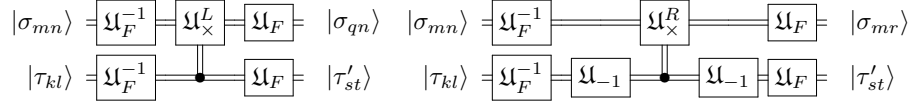


FIG. 7. Quantum circuits implementing Clebsch-Gordan sums for generic finite groups. (left) \mathfrak{U}_{CG}^L and (right) \mathfrak{U}_{CG}^R

and let $h' = gh$, Eq. (C3) can be simplified as

$$\hat{P}_{\sigma'_{sq}}(\mathbf{x})\hat{\Gamma}_{\sigma,m,n}(\mathbf{x},i)\hat{P}_0(\mathbf{x}) = \frac{\sqrt{d_\sigma}}{|G|^2} \sum_g \Gamma_{sq}^{(\sigma')}(g^{-1}) \sum_k \Gamma_{mk}^{(\sigma)}(g^{-1})^* \sum_{h'} \left(\hat{R}_{h'-1} \begin{array}{c} \hat{L}_{h'} \\ | \mathbf{x} \rangle \\ \hat{R}_{h'-1} \end{array} \hat{\Gamma}_{\sigma,k,n} \hat{L}_{h'} \right). \quad (\text{C5})$$

Using the orthogonality Eq. (B4), we get

$$\hat{P}_{\sigma'_{sq}}(\mathbf{x})\hat{\Gamma}_{\sigma,m,n}(\mathbf{x},i)\hat{P}_0(\mathbf{x}) = \delta_{\sigma'\sigma} \delta_{sm} d_\sigma^{-1/2} \hat{\Gamma}_{\sigma,q,n}(\mathbf{x},i)\hat{P}_0(\mathbf{x}). \quad (\text{C6})$$

Similarly for $(\mathbf{x} + \mathbf{i})$ at the other end of the erroneous link,

$$\hat{R}_{g^{-1}}\hat{\Gamma}_{\sigma,m,n} = \sum_k \Gamma_{kn}^{(\sigma)}(g)^* \hat{\Gamma}_{\sigma,m,k} \hat{R}_{g^{-1}}, \quad (\text{C7})$$

and

$$\hat{P}_{\sigma''_{tr}}(\mathbf{x} + \mathbf{i})\hat{\Gamma}_{\sigma,q,n}(\mathbf{x},i)\hat{P}_0(\mathbf{x} + \mathbf{i}) = \delta_{\sigma''\sigma} \delta_{tn} d_\sigma^{-1/2} \hat{\Gamma}_{\sigma,q,r}(\mathbf{x},i)\hat{P}_0(\mathbf{x} + \mathbf{i}). \quad (\text{C8})$$

Combining Eq. (C6) and Eq. (C8) gives

$$\hat{P}_{\sigma''_{tr}}(\mathbf{x} + \mathbf{i})\hat{P}_{\sigma'_{sq}}(\mathbf{x})\hat{\Gamma}_{\sigma,m,n}(\mathbf{x},i)\hat{P}_0(\mathbf{x})\hat{P}_0(\mathbf{x} + \mathbf{i}) = \delta_{\sigma,\sigma'} \delta_{\sigma''\sigma} \delta_{sm} \delta_{tn} \frac{1}{d_\sigma} \hat{\Gamma}_{\sigma,q,r}(\mathbf{x},i)\hat{P}_0(\mathbf{x})\hat{P}_0(\mathbf{x} + \mathbf{i}). \quad (\text{C9})$$

Using the fact $\hat{P}_0(\mathbf{x})\hat{P}_0(\mathbf{x} + \mathbf{i})|\Psi\rangle_{\text{inv}} = |\Psi\rangle_{\text{inv}}$, the outcome of \mathcal{U}_{dec} the gauge field state $\hat{\Gamma}_{\sigma,m,n}(\mathbf{x},i)|\Psi\rangle_{\text{inv}}$ is

$$\begin{aligned} & \sum_{\sigma'_{sq}, \sigma''_{tr}} \hat{P}_{\sigma''_{tr}}(\mathbf{x} + \mathbf{i})\hat{P}_{\sigma'_{sq}}(\mathbf{x})\hat{\Gamma}_{\sigma,m,n}(\mathbf{x},i)|\Psi\rangle_{\text{inv}} \otimes |\sigma'_{sq}(\mathbf{x})\rangle \otimes |\sigma''_{tr}(\mathbf{x} + \mathbf{i})\rangle \\ &= \sum_{q,r} \frac{1}{d_\sigma} \hat{\Gamma}_{\sigma,q,r}(\mathbf{x},i)|\Psi\rangle_{\text{inv}} \otimes |\sigma'_{sq}(\mathbf{x})\rangle \otimes |\sigma''_{tr}(\mathbf{x} + \mathbf{i})\rangle \end{aligned} \quad (\text{C10})$$

Appendix D: Clebsch-Gordan sum in the group element basis

The relation between Clebsch-Gordan coefficients and matrix elements of the representations [109] is :

$$\frac{d_{\sigma''}}{|G|} \sum_{g \in G} \Gamma_{mn}^{(\sigma)}(g) \Gamma_{kq}^{(\sigma')}(g) \Gamma_{lr}^{(\sigma'')}(g)^* = \sum_{\alpha} \langle \sigma''_r, \alpha | \sigma_n, \sigma'_q \rangle \langle \sigma_m, \sigma'_k | \sigma''_l, \alpha \rangle. \quad (\text{D1})$$

The Clebsch-Gordan coefficients satisfy $\langle \sigma_n, \sigma'_q | \sigma''_r, \alpha \rangle^* = \langle \bar{\sigma}_n, \bar{\sigma}'_q | \bar{\sigma}''_r, \alpha \rangle$. We can also choose the phases of representation to satisfy $\langle \sigma''_r, \alpha | \sigma_n, \sigma'_q \rangle = \langle \sigma_n, \sigma'_q | \sigma''_r, \alpha \rangle^*$, which will be used for later discussions.

With Eq. (D1), we show that the group multiplications Fourier transformed to the representation basis is equivalent to the addition of representations according to the Clebsch-Gordan coefficients (Fig. 7).

$$\begin{aligned} \mathfrak{U}_{CG}^L &= \frac{\sqrt{d_\sigma d_{\sigma'_1} d_\tau d_{\tau'}}}{|G|^2} \Gamma_{qr}^{(\sigma')}(g_2 g_1) \Gamma_{st}^{(\tau')}(g_2) \Gamma_{mn}^{(\sigma)}(g_1)^* \Gamma_{kl}^{(\tau)}(g_2)^* (|\sigma'_{qr}\rangle \otimes |\tau'_{st}\rangle \langle \sigma_{mn}| \otimes \langle \tau_{kl}|) \\ &= \frac{\sqrt{d_\sigma d_{\sigma'_1} d_\tau d_{\tau'}}}{|G|^2} \Gamma_{qu}^{(\sigma')}(g_2) \Gamma_{ur}^{(\sigma')}(g_1) \Gamma_{st}^{(\tau')}(g_2) \Gamma_{mn}^{(\sigma)}(g_1)^* \Gamma_{kl}^{(\tau)}(g_2)^* (|\sigma'_{qr}\rangle \otimes |\tau'_{st}\rangle \langle \sigma_{mn}| \otimes \langle \tau_{kl}|) \end{aligned} \quad (\text{D2})$$

where all the indices for group elements and group representations are summed over. Use the orthogonality Eq. (B4) to sum g_1 , giving

$$\begin{aligned}\mathfrak{U}_{CG}^L &= \frac{\sqrt{d_\tau d_{\tau'}}}{|G|} \Gamma_{qm}^{(\sigma)}(g_2) \Gamma_{st}^{(\tau')}(g_2) \Gamma_{kl}^{(\tau)}(g_2)^* (|\sigma_{qn}\rangle \otimes |\tau'_{st}\rangle \langle \sigma_{mn}| \otimes \langle \tau_{kl}|) \\ &= \frac{\sqrt{d_\tau d_{\tau'}}}{|G|} [\Gamma_{qm}^{(\bar{\sigma})}(g_2) \Gamma_{st}^{(\tau')}(g_2)^* \Gamma_{kl}^{(\tau)}(g_2)]^* (|\sigma_{qn}\rangle \otimes |\tau'_{st}\rangle \langle \sigma_{mn}| \otimes \langle \tau_{kl}|),\end{aligned}\quad (\text{D3})$$

Finally apply Eq. (D1) and convert the product of matrix elements to the Clebsch-Gordan coefficients,

$$\begin{aligned}\mathfrak{U}_{CG}^L &= \sqrt{d_\tau/d_{\tau'}} (\langle \tau'_t, \alpha | \bar{\sigma}_m, \bar{\tau}_l \rangle \langle \bar{\sigma}_q, \bar{\tau}_k | \tau'_s, \alpha \rangle)^* (|\sigma_{qn}\rangle \otimes |\tau'_{st}\rangle \langle \sigma_{mn}| \otimes \langle \tau_{kl}|) \\ &= \sqrt{d_\tau/d_{\tau'}} \langle \bar{\tau}'_t, \alpha | \sigma_m, \bar{\tau}_l \rangle \langle \sigma_q, \bar{\tau}_k | \bar{\tau}'_s, \alpha \rangle (|\sigma_{qn}\rangle \otimes |\tau'_{st}\rangle \langle \sigma_{mn}| \otimes \langle \tau_{kl}|)\end{aligned}\quad (\text{D4})$$

Thus through \mathfrak{U}_{CG}^L , σ in register 1 stays the same and τ in register 2 changes into τ' .

Thus, \mathfrak{U}_{CG}^L “adds” the left vector in register 1 to register 2 according to the Clebsch-Gordan coefficients. For register 1, the process preserves quantum numbers σ, n but not necessarily m when the representation σ is not one-dimensional. The old flux σ_m is added to $\bar{\tau}_l$ and the new flux σ_q to $\bar{\tau}_k$. Similarly, \mathfrak{U}_{CG}^R adds the right-vector in register 1 to register 2:

$$\begin{aligned}\mathfrak{U}_{CG}^R &= \frac{\sqrt{d_\sigma d_{\sigma'} d_\tau d_{\tau'}}}{|G|^2} \Gamma_{qr}^{(\sigma')}(g_1 g_2^{-1}) \Gamma_{st}^{(\tau')}(g_2) \Gamma_{mn}^{(\sigma)}(g_1)^* \Gamma_{kl}^{(\tau)}(g_2)^* (|\sigma'_{qr}\rangle \otimes |\tau'_{st}\rangle \langle \sigma_{mn}| \otimes \langle \tau_{kl}|) \\ &= \sqrt{d_\tau/d_{\tau'}} \langle \sigma_n, \tau_l | \tau'_t, \alpha \rangle \langle \tau'_s, \alpha | \sigma_r, \tau_k \rangle (|\sigma_{mr}\rangle \otimes |\tau'_{st}\rangle \langle \sigma_{mn}| \otimes \langle \tau_{kl}|)\end{aligned}\quad (\text{D5})$$

Appendix E: Correctable errors and independence polynomials

In this appendix, we explain our methods to compute Q_n – the number of possible ways to arrange n links with correctable errors in the lattice, such that the correctability condition is still satisfied, with tools of graph theory [112]. The method can be applied to lattices of generic shapes.

A graph consists of vertices and edges. An *independent subset* of vertices is a set of vertices in which no two vertices are adjacent to the same edge. The *independence polynomial* of a graph is

$$I(z) = \sum_n a_n z^n, \quad (\text{E1})$$

where a_n is the number of different independent subsets of n vertices in the graph.

For a finite lattice \mathfrak{L} , we create a corresponding graph \mathfrak{L}' in the following way:

- convert each link of \mathfrak{L} into a vertex of \mathfrak{L}' ;
- for each pair of vertices in \mathfrak{L}' , create an edge adjacent to them, if the Γ_σ -type errors that occur simultaneously to the corresponding links in \mathfrak{L} can break the correctability condition.

Thus, each way of arranging n erroneous links to satisfy the correctability condition corresponds to an independent subset of vertices in the new graph. This implies that Q_n is the number independent subsets of n vertices in the new graph and Ξ the independence polynomial.

For each lattice considered in Fig. 5 and Fig. 6, we construct the adjacency matrix of the corresponding graph \mathfrak{L}' – an $N_L \times N_L$ matrix in which the element in row i and column j is 0 if the i, j -th vertices are independent, and 1 if they are adjacent to the same edge. We then use the Python library `hobj` [112] to compute the coefficients of the independence polynomials from the adjacent matrices. The connectivity for the MED condition would be higher than that for the KL condition.